Geophysical Journal International

Geophys. J. Int. (2016) **207,** 317–332
Advance Access publication 2016 July 27
GJI Geodynamics and tectonics

doi: 10.1093/gji/ggw276

High-resolution estimates of Nubia–Somalia plate motion since 20 Ma from reconstructions of the Southwest Indian Ridge, Red Sea and Gulf of Aden

C. DeMets[1] and S. Merkouriev[2,3]

[1] *Department of Geoscience, University of Wisconsin-Madison, Madison, WI* 53706, *USA. E-mail: chuck@geology.wisc.edu*
[2] *Pushkov Institute of Terrestrial Magnetism of the Russian Academy of Sciences, St. Petersburg Filial.* 1 *Mendeleevskaya Liniya, St. Petersburg* 199034, *Russia*
[3] *Institute of Earth Sciences, St. Petersburg State University, Universitetskaya nab.,* 7-9, *St. Petersburg* 199034, *Russia*

Accepted 2016 July 21. Received 2016 May 16; in original form 2016 January 12

SUMMARY

Large gaps and inconsistencies remain in published estimates of Nubia–Somalia plate motion based on reconstructions of seafloor spreading data around Africa. Herein, we use newly available reconstructions of the Southwest Indian Ridge at ∼1-Myr intervals since 20 Ma to estimate Nubia–Somalia plate motion farther back in time than previously achieved and with an unprecedented degree of temporal resolution. At the northern end of the East African rift, our new estimates of Nubia–Somalia motion for six times from 0.78 Ma to 5.2 Ma differ by only 2 per cent from the rift-normal component of motion that is extrapolated from a recently estimated GPS angular velocity. The rate of rift-normal extension thus appears to have remained steady since at least 5.2 Ma. Our new rotations indicate that the two plates have moved relative to each other since at least 16 Ma and possibly longer. Motion has either been steady since at least 16 Ma or accelerated modestly between 6 and 5.2 Ma. Our Nubia–Somalia rotations predict 42.5 ± 3.8 km of rift-normal extension since 10.6 Ma across the well-studied, northern segment of the Main Ethiopian Rift, consistent with 40–50 km estimates for extension since 10.6 Myr based on seismological surveys of this narrow part of the plate boundary. Nubia–Somalia rotations are also derived by combining newly estimated Somalia–Arabia rotations that reconstruct the post-20-Ma opening of the Gulf of Aden with Nubia–Arabia rotations estimated via a probabilistic analysis of plausible opening scenarios for the Red Sea. These rotations predict Nubia–Somalia motion since 5.2 Myr that is consistent with that determined from Southwest Indian Ridge data and also predict 40 ± 3 km of rift-normal extension since 10.6 Ma across the Main Ethiopian Rift, consistent with our 42.5 ± 3.8 km Southwest Indian Ridge estimate. Our new rotations exclude at high confidence level previous estimates of 12 ± 13 and 123 ± 14 km for rift-normal extensions across the Main Ethiopian Rift since 10.6 Ma based on reconstructions of Chron 5n.2 along the Southwest Indian Ridge. Sparse coverage of magnetic reversals older than 16 Ma along the western third of the Southwest Indian Ridge precludes reliable determinations of Nubia–Somalia plate motion before 16 Ma, leaving unanswered the key question of when the motion between the two plates began.

Key words: Plate motions; Continental tectonics: extensional; Africa.

1 INTRODUCTION AND BACKGROUND

The Cenozoic collision of continental Africa and Eurasia during the closure of the Neo-Tethys Ocean altered the kinematic and tectonic evolution of the Africa plate, including a slowdown in Africa's northward motion relative to its surrounding plates (e.g. Rosenbaum *et al.* 2002; McQuarrie *et al.* 2003; Patriat *et al.* 2008; Cande *et al.* 2010; Reilinger & McClusky 2011) and an accompanying fragmentation of the plate into distinct Arabia, Nubia and Somalia plates (Fig. 1). Fragmentation of the Africa plate began at 29–24 Ma, when incipient rifting along the present Gulf of Aden and Red Sea signalled the break-off of the Arabian peninsula from Africa (e.g. Bosworth *et al.* 2005; Wolfenden *et al.* 2005). Motion between eastern and western Africa (Somalia and Nubia, respectively) may have started at the same time or could conceivably have started as recently as 11–10 Ma, when rifting along the northern end of the East

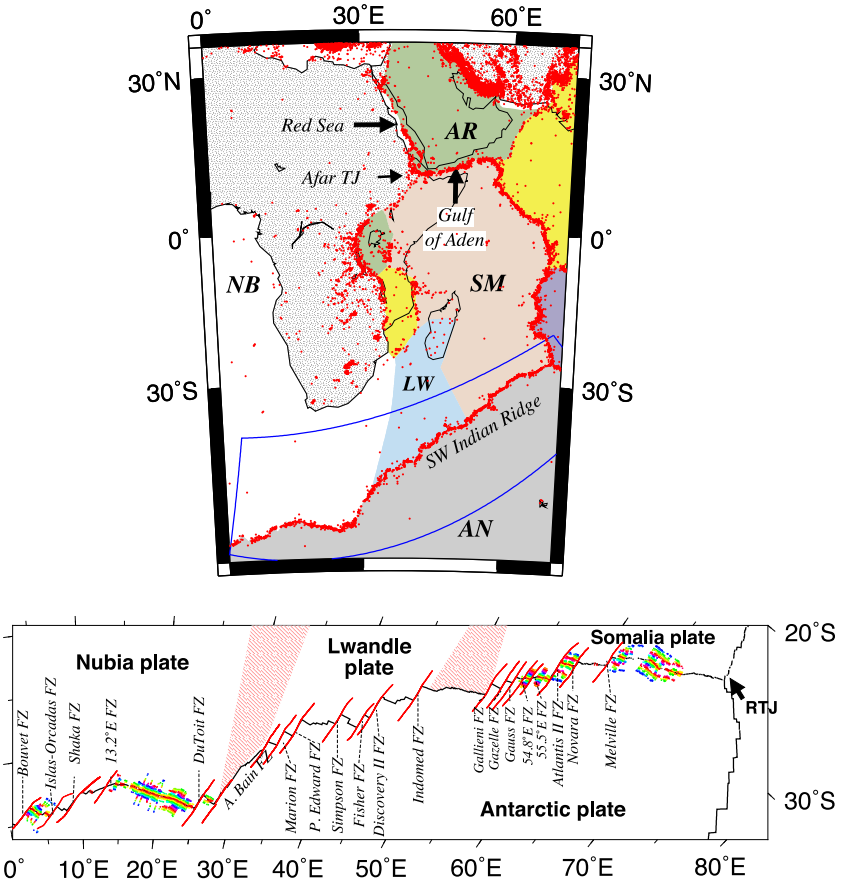

Figure 1. Location map for study area. Upper map shows plate tectonic setting of the study area, and earthquakes from 1964 through 2013 shallower than 60 km and with magnitudes over 3.5 (red circles). The blue rectangle delimits the region shown in the lower map. Lower map is an oblique Mercator projection of the Southwest Indian Ridge with prominent fracture zones labelled. Coloured circles show crossings of transform faults, fracture zones and magnetic reversals 1n (0.78 Ma) to 6n(o) (19.72 Ma) from DeMets *et al.* (2015) that are used here to estimate Nubia–Somalia plate rotations. Abbreviations—AN, Antarctic Plate; AR, Arabia Plate; LW, Lwandle Plate; NB, Nubia Plate; RTJ, Rodrigues triple junction; SM, Somalia Plate; TJ, triple junction. Earthquakes are for the period 1964–2013, are limited to magnitudes greater than 3.5 and depths above 60 km (www.neic.cr.usgs.gov).

African Rift created the modern Afar triple junction (e.g. Wolfenden *et al.* 2004; Keranen & Klemperer 2008; Corti 2009).

In this study, we quantify motion between the Nubia and Somalia plates during the Neogene and Quaternary, a topic relevant to studies of rifting in eastern Africa and reconstructions of global plate motions. Numerous authors have estimated Nubia–Somalia plate rotations from Arabia–Somalia and Nubia–Arabia plate rotations that reconstruct the respective opening histories of the Gulf of Aden and Red Sea (e.g. Freund 1970; Mohr 1970; McKenzie *et al.* 1970; Le Pichon & Francheteau 1978; Joffe & Garfunkel 1987; Jestin *et al.* 1994; Garfunkel & Beyth 2006; Iaffaldano *et al.* 2014a). Their utility is however limited by the low fidelity of the seafloor spreading magnetic lineations in the Red Sea and Gulf of Aden and absence of any readily identifiable Red Sea magnetic lineations that are older than ∼5–7 Ma (Roeser 1975; Cochran 1983; Izzeldin 1987).

Nubia–Somalia plate motion can also be estimated from rotations that reconstruct Nubia–Antarctic and Somalia-Antarctic plate motions across the ∼8000-km long, ultraslow-spreading Southwest Indian Ridge (Fig. 1), where an abundance of fracture zones and magnetic lineations can be used to estimate the long-term plate motions. Although early efforts to do so were unsuccessful due to sparse data coverage and the low fidelity of the Southwest Indian Ridge magnetic anomalies (e.g. Minster *et al.* 1974; Minster & Jordan 1978; DeMets *et al.* 1990; Jestin *et al.* 1994), more recent efforts have been increasingly successful. Chu & Gordon (1999) were the first to show that Nubia–Somalia plate motion is statistically resolvable from 3-Myr average seafloor spreading rates well distributed along the Southwest Indian Ridge and that the boundary between the two plates intersects the ridge in the vicinity of the Andrew Bain fracture zone. Horner-Johnson *et al.* (2005) use an improved set of 3-Myr-average plate kinematic data to refine Chu & Gordon's results and Horner-Johnson *et al.* (2007) described the first kinematic evidence and rotation estimates for the Lwandle plate north of the ridge (Fig. 1). Stamps *et al.* (2008) show that GPS measurements of instantaneous motion between Nubia and Somalia are consistent with motion between the two plates over the past 3 Myr, suggesting that their relative motion has remained steady since at least 3 Myr.

Less is known with any confidence about Nubia–Somalia motion before 3 Ma as determined from data along the Southwest Indian Ridge. From reconstructions of Chron 5n.2 along the ridge, a 11-Myr Nubia–Somalia rotation estimated by Lemaux *et al.* (2002) predicts 23 ± 6 km of opening at the northern end of the East African rift in a direction ∼ 60° oblique to the rift. In contrast, a 11-Myr (C5n.2) rotation estimated by Royer *et al.* (2006) predicts 130 ± 31 km of opening nearly orthogonal to the rift. The two estimates differ by ∼500 per cent.

Herein, we estimate Nubia–Somalia motion since 20 Ma from newly available rotations that reconstruct at ∼1-Myr intervals the seafloor spreading history of the Southwest Indian Ridge since 20 Ma (DeMets, Merkouriev & Sauter 2015; hereafter abbreviated DMS15). Our analysis is presented in several stages. In the first half of the analysis, we compare the motions predicted by Nubia–Somalia rotations that we estimate from closure of the Nubia–Antarctic–Somalia plate circuit (i.e. the Southwest Indian Ridge) with estimates from Global Positioning System (GPS) measurements at sites on the Nubia and Somalia plates (e.g. Stamps *et al.* 2008; Saria *et al.* 2014) and plate kinematic data that average motion over the past 3 Myr (e.g. Horner-Johnson *et al.* 2005, 2007; DeMets *et al.* 2010). We then extend the analysis to progressively older times in order to test the accuracy of the new rotations against an assortment of independent estimates and identify any significant changes in motion, including the possibility that motion between the two plates began during the past 20 Myr.

In the latter part of the analysis we estimate Nubia–Somalia rotations from reconstructions of the seafloor spreading histories of the Gulf of Aden and Red Sea, with a goal of evaluating their consistency or lack thereof with the rotations determined from data along the Southwest Indian Ridge. Motion between Arabia and Somalia is estimated from reconstructions of eight well-mapped magnetic reversals between Chron 2An.1 (2.58 Ma) and Chron 6n (19.72 Ma) in the Gulf of Aden (Fournier *et al.* 2010). Similarly detailed estimates of Nubia–Arabia motion are not available due to the absence of easily identified magnetic reversals older than ∼5 Ma in the Red Sea. To overcome this, we use a probabilistic procedure to identify all two-stage Nubia–Arabia opening models that satisfy geologic, geodetic and plate kinematic constraints on the opening of the Red Sea. These include constraints on the opening age of the Red Sea, constraints on when motion between Nubia and Arabia may have changed during the past 20 Myr, structural constraints on the offset of the Dead Sea Fault and extension across the Gulf of Suez and geological constraints on the total opening pole and angle for the Red Sea (e.g. McKenzie *et al.* 1970; Joffe & Garfunkel 1987; Sultan *et al.* 1992; Garfunkel & Beyth 2006).

2 NUBIA–SOMALIA ROTATIONS FROM SOUTHWEST INDIAN RIDGE DATA

We begin by estimating Nubia–Somalia rotations from rotations that reconstruct the post-20 Myr motions of the Somalia-Antarctic and Nubia–Antarctic plate pairs across the Southwest Indian Ridge (DeMets *et al.* 2015). For the Somalia–Antarctic plate pair, DMS15 invert 3645 crossings of magnetic reversals, fracture zones and transform faults to estimate best-fitting finite rotations for 21 distinct times since 20 Ma. These data extend west from the Rodrigues triple junction at ∼70°E to the Gallieni fracture zone (∼52°E) (Fig. 1), the approximate western limit of the Somalia plate north of the ridge. For the Nubia–Antarctic plate pair, DMS15 invert 3574 observations between the Bouvet triple junction and Andrew Basin transform fault (Fig. 1) to estimate best-fitting finite rotations at 19 times during the past 20 Ma. Insufficient ship- and airborne-survey coverage of magnetic reversals 5D and 5E precluded any estimates of Nubia–Antarctic and hence Nubia–Somalia finite rotations for those two times. Readers are referred to DMS15 for further information about the underlying data.

Two sequences of rotations for each of the Nubia–Antarctic and Somalia-Antarctic plate pairs are used herein, all from DMS15. One, which we refer to hereafter as best-fitting rotations, optimally reconstructs data from the Southwest Indian Ridge in a best-fitting, least-squares sense. Iaffaldano *et al.* (2012) show that angular velocities that are differentiated from closely spaced, best-fitting rotations often predict erratic, geodynamically implausible changes in plate motion. DMS15 thus also extracted less noisy rotation sequences for both plate pairs by applying a Bayesian method encoded in REDBACK software (Iaffaldano *et al.* 2014b) to their original, best-fitting rotations. The misfits of these noise-reduced rotations (which are found in supplemental tables 1 and 3 in DMS15) to the Southwest Indian Ridge magnetic reversal and fracture zone crossings are typically no more than a few hundred meters larger than the misfits of the best-fitting rotations. DMS15 interpret these increases in misfit as insignificant, thereby setting the stage for using noise-reduced rotations for this analysis.

We determined Nubia–Somalia rotations for the 19 times that are common to the Nubia–Antarctica and Somalia-Antarctica plate pairs using standard methods for combining finite rotations and their covariances (Kirkwood *et al.* 1999). Table 1 and Supporting Information Table S1 give Nubia–Somalia rotations and uncertainties that we determined from the noise-reduced and best-fitting rotations for the Nubia–Antarctica and Somalia-Antarctica plate pairs, respectively. The noise-reduced Nubia–Somalia rotations in Table 1 were estimated by combining the noise-reduced Nubia–Antarctic and Somalia-Antarctic rotations rather than applying the REDBACK software to the best-fitting sequence of Nubia–Somalia rotations in Supporting Information Table S1.

Fig. 2 compares the best-fitting and noise-reduced estimates of the Nubia–Somalia finite rotation poles (Figs 2a and b) and angles (Fig. 2c). As might be expected, the noise-reduced poles are clustered more tightly than are the best-fitting poles, which follow an irregular path and are scattered broadly within the mapped area (Fig. 2a). The variance of the noise-reduced rotation angles with respect to a simple linear angle-change model is ∼90 per cent less than for the best-fitting angles (Fig. 2c), consistent with a simpler history of relative motion between Nubia and Somalia than is implied by the best-fitting estimates.

Differentiation of the finite rotations in Table 1 gives a sequence of interval angular velocities (Table 2) that predict in detail the evolution since 20 Ma of Nubia–Somalia velocities everywhere along their plate boundary. At a location along the northern end of the Nubia–Somalia plate boundary, these angular velocities predict interval rates of 4 ± 1 mm yr^{-1} of opening since ∼12 Ma and 5–6 mm yr^{-1} from 20 to 12 Ma (Fig. 3a). The predicted slip directions vary $\pm$ 10° about their mean value for nearly all of the past 20 Myr (Fig. 3b), except before 18.5 Ma, when the predicted slip direction was highly oblique to the present-day East African Rift. For comparison, the best-fitting interval rates and directions (not shown) vary erratically between 1 and 13 mm yr^{-1} and span a 180-degree range.

Given the insignificant fitting penalty that is associated with the noise-reduced versus the best-fitting rotations (see above) and the simpler evolution of the predicted interval velocities for the former versus the latter, all subsequent results are based on the noise-reduced rotations in Table 1 and angular velocities in Table 2.

3 MOTION SINCE 20 MA AND COMPARISONS TO INDEPENDENT CONSTRAINTS

We now evaluate the accuracy of our newly estimated rotations via a comparison of their predictions to a variety of independent

Table 1. Nubia–Somalia noise-reduced rotations from Southwest Indian Ridge.

Chron	Age (Ma)	Lat. (°N)	Long. (°E)	Ω (°)	Covariances					
					a	*b*	*c*	*d*	*e*	*f*
1n	0.781	−40.12	3.22	0.035	56.7	−36.2	−43.3	23.7	28.5	34.5
2n	1.778	−43.11	4.70	0.081	71.1	−45.4	−54.5	29.9	36.2	44.0
2An.1	2.581	−44.71	5.23	0.121	85.8	−54.6	−65.5	36.1	43.8	53.4
2An.3	3.596	−45.44	5.06	0.172	110.6	−70.1	−84.3	46.5	56.6	69.2
3n.1	4.187	−45.41	4.53	0.199	130.6	−82.7	−99.5	55.0	67.1	82.2
3n.4	5.235	−45.40	4.20	0.235	156.7	−101.2	−122.5	68.2	83.6	102.8
3An.1	6.033	−45.77	5.46	0.254	206.6	−132.8	−160.7	88.4	108.1	132.6
3An.2	6.733	−45.81	6.76	0.275	262.6	−166.5	−201.0	109.1	132.9	162.5
4n.1	7.528	−45.44	7.86	0.307	274.1	−172.3	−207.8	112.4	137.1	167.8
4n.2	8.108	−45.12	8.63	0.332	272.3	−169.7	−204.4	110.4	134.7	165.2
4A	9.105	−44.79	10.57	0.381	254.4	−153.9	−184.2	98.4	119.9	147.1
5n.1	9.786	−44.63	11.78	0.417	250.6	−148.3	−176.4	94.0	114.6	141.0
5n.2	11.056	−44.20	10.85	0.464	235.6	−135.7	−160.7	84.4	102.5	125.7
5An.2	12.474	−43.75	9.21	0.522	230.0	−129.2	−152.0	80.4	97.9	120.6
5AC	13.739	−43.80	9.22	0.599	208.7	−114.9	−134.3	73.7	90.6	113.1
5AD	14.609	−44.10	9.91	0.658	224.1	−119.4	−138.3	77.4	95.5	120.3
5Cn.1	15.974	−44.83	11.28	0.757	358.5	−179.2	−205.7	109.8	134.7	168.8
6ny	18.748	−43.80	14.60	0.897	431.5	−196.8	−221.3	127.6	160.9	209.1
6no	19.722	−44.39	7.68	0.807	351.9	−176.0	−201.7	121.2	156.9	211.1

These rotations reconstruct movement of the Somalia plate relative to the Nubia plate and are determined from combining Nubia–Antarctica and Somalia–Antarctica noise-reduced rotations from tables S1 and S2 of DeMets *et al.* (2015). Rotation angles Ω are positive anticlockwise. Magnetic reversal ages are adopted from the astronomically tuned GTS12 timescale (Hilgen *et al.* 2012; Ogg 2012). The Cartesian rotation covariances are calculated in a Somalia-fixed reference frame and have units of 10^{-9} radians^2. Elements *a*, *d* and *f* are the variances of the (0°N, 0°E), (0°N, 90°E) and 90°N components of the rotation. The covariance matrices are reconstructed as follows:

$$\begin{pmatrix} a & b & c \\ b & d & e \\ c & e & f \end{pmatrix} \quad (1)$$

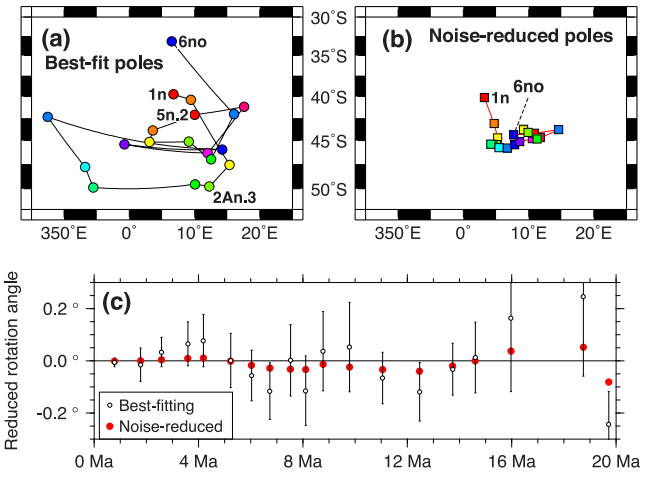

Figure 2. Comparison of Nubia–Somalia plate motion poles and angles before and after noise reduction with REDBACK software described in the text. (a) Best-fitting finite-rotation poles (Table 2). (b) Noise-reduced poles (Table 1). Pole error ellipses are omitted for clarity. (c) Best-fitting and noise-reduced opening angles reduced by a slope of 0.045° Myr^{-1}.

estimates that span timescales from the present-day (Section 3.2) to the past 10.6 Ma (Section 3.3). We focus in particular on comparing estimates of plate motion across the well-studied northern segment of the Main Ethiopian Rift, where the Nubia–Somalia plate boundary is narrow enough to allow for meaningful comparisons of far-field plate motions to near-field estimates derived from seismic, structural, or other localized studies (Corti 2009). We leave comparisons at locations farther south, where the rift bifurcates into eastern and western segments and deformation is spread across a broad area, to other authors. Given the importance of the Main Ethiopian Rift to the remainder of the study, we first summarize the relevant near-field structural and age constraints at this locale.

3.1 Independent constraints from the Main Ethiopian Rift

The Main Ethiopian Rift is located at the northern end of the East Africa Rift system, where the narrow Ethiopian rift opens northeastwards into the triangular-shaped Afar depression (Fig. 4a). The rift consists of structurally distinct northern, central and southern segments that appear to have activated at different times and which may represent different stages of continental extension (Hayward & Ebinger 1996; Bonini *et al.* 2005; Corti 2009; Abebe *et al.* 2010). A variety of observations summarized below provide useful information about the movement across the rift back to 10.6 Ma.

3.1.1 Quaternary extension direction

Structural data, stratigraphic relations and radiometric ages of the volcanics in the northern rift segment indicate that extension began there at ∼10.6 Ma (Wolfenden *et al.* 2004), since which most or all of the extension has been accommodated by a combination of faulting and magmatic intrusion/extrusion within the rift valley and along its border faults (Wolfenden *et al.* 2004). Estimates of the recent opening direction across the northern rift valley from earthquake focal mechanisms (Keir *et al.* 2006), fault planes and fault lineations (Pizzi *et al.* 2006), volcano shapes (Casey *et al.* 2006) and GPS measurements at sites bounding the rift valley (Bendick *et al.* 2006) range from N95°E-N105°E (Fig. 4a). These agree well with the N100°–113°E range of principal minimum stress directions

Table 2. Nubia–Somalia noise-reduced angular velocities.

Age(o) (Ma)	Age(y) (Ma)	Lat. (°N)	Long. (°E)	$\dot{\omega}$ (° Myr^{-1})	Covariances					
					a	*b*	*c*	*d*	*e*	*f*
0.781	0.00	−46.45	10.66	0.039	5.69	−4.41	−5.61	3.51	4.51	5.82
1.778	0.781	−43.06	2.33	0.047	7.23	−5.59	−7.12	4.45	5.71	7.35
2.581	1.778	−47.17	9.88	0.052	12.14	−9.31	−11.83	7.36	9.43	12.11
3.596	2.581	−49.22	9.62	0.050	8.30	−6.31	−8.00	4.94	6.32	8.11
4.187	3.596	−47.31	4.64	0.045	26.89	−20.17	−25.49	15.64	19.94	25.50
5.235	4.187	−43.03	357.56	0.038	9.29	−6.88	−8.68	5.28	6.72	8.56
6.033	5.235	−34.99	354.67	0.033	17.41	−12.77	−16.05	9.69	12.28	15.60
6.733	6.033	−34.55	2.94	0.034	24.84	−18.06	−22.63	13.55	17.12	21.67
7.528	6.733	−41.58	16.41	0.041	20.90	−15.08	−18.87	11.22	14.15	17.89
8.108	7.528	−42.87	23.80	0.042	42.16	−30.17	−37.72	22.32	28.13	35.53
9.105	8.108	−43.96	28.48	0.050	14.99	−10.65	−13.31	7.85	9.89	12.50
9.786	9.105	−40.47	23.02	0.049	33.27	−23.51	−29.38	17.28	21.80	27.56
11.056	9.786	−39.17	4.39	0.032	9.77	−6.87	−8.60	5.05	6.39	8.09
12.474	11.056	−47.53	8.70	0.040	7.92	−5.53	−6.91	4.04	5.10	6.45
13.739	12.474	−50.47	22.01	0.061	10.05	−6.89	−8.56	4.94	6.19	7.78
14.609	13.739	−51.24	25.03	0.070	21.27	−14.30	−17.64	10.09	12.58	15.72
15.974	14.609	−53.67	23.52	0.072	8.71	−5.75	−7.08	4.02	5.01	6.25
18.748	15.974	−37.19	20.75	0.055	2.09	−1.33	−1.63	0.92	1.14	1.43
19.722	18.748	−27.99	74.44	−0.113	18.98	−11.43	−13.99	7.66	9.62	12.16

These angular velocities specify the forward motion of the Nubia plate relative to the Somalia plate during the time period given in the first two columns. The angular rotation rates $\dot{\omega}$ are positive anticlockwise for the old to the young limit of each time interval. The angular velocities and covariances are calculated in a Somalia-fixed reference frame. The covariances, which were derived from the REDBACK angular velocity covariances for the Nubia–Antarctic and Somalia-Antarctic plate pairs, have units of 10^{-7} radians^2 Myr^{-2}.

estimated by Philippon *et al.* (2014) from palaeostress inversions of fault plane and lineation measurements from the nearby southern rift segment (arrow labelled 'd' in Fig. 4a) and an N105°E extension direction estimated by Corti *et al.* (2013) from structural observations along the western margin of the southern rift segment. The Quaternary opening direction across the Main Ethiopian Rift thus appears to be reliably determined.

3.1.2 Cumulative plate separation since 10.6 Ma

The total extension across the northern rift segment since it began opening at 10.6 Ma can be approximated from differences in the thicknesses of the crust within the rift and along its undeformed borders (Corti 2009). Dense seismic surveys of the rift and its shoulders give average depths to Moho of 26 km below much of the northernmost rift (Maguire *et al.* 2006) and 41–42 km below the unextended crust outside the rift valley (Cornwell *et al.* 2010). These imply a stretching factor of ∼1.6 (i.e. the original crustal thickness divided by the final thickness) in the unlikely case that all of the extension since 10.6 Ma has occurred via faulting within the rift or on its border faults. A stretching factor of 1.6 implies total rift-normal opening of 37 km for the ∼100-km wide northern segment. This constitutes a minimum estimate for the rift-normal extension, which we round hereafter to 40 km.

A more realistic estimate of the total extension across the northern rift segment accounts for new lithosphere that has accreted within the rift valley since 10.6 Ma via magmatic diking and lithospheric underplating. 3-D seismic imaging of the northern rift and its adjacent unrifted areas reveals 20-km wide, 50-km long, high-velocity features below the ≈20-km wide Wonji volcanic/fault belt near the axis of the rift valley (Keranen *et al.* 2004). These are interpreted as cooled mafic intrusions (Keranen *et al.* 2004), consistent with other evidence that extension within the Wonji fault belt is accommodated by pervasive diking at depth, magmatic intrusion and slip along the numerous, closely spaced, low-offset normal faults that define the belt (Ebinger & Casey 2001, Casey *et al.* 2006 and other references in Corti 2009).

If we simplistically assume that the entire 20-km-wide Wonji volcanic belt consists of newly accreted lithosphere and the remaining 80 km of the 100-km-wide rift was formed by extensional faulting, the net implied extension is 50 km for a stretching factor of 1.6. The estimated plate separations thus range from a 40-km minimum to a more realistic 50 km since 10.6 Ma.

3.2 Geologically recent motion: 3.6 Ma to present

3.2.1 Comparison to GPS and neotectonic estimates

Fig. 4 compares Nubia–Somalia plate velocities within the Main Ethiopian Rift as estimated from the angular velocities in Table 2 and from structural observations summarized in Section 3.1.1 (Fig. 4a) and geodetic angular velocities described below (Fig. 4b).

Recent estimates of the Nubia–Somalia angular velocity from inversions of GPS site velocities widely distributed on the two plates include those of Stamps *et al.* (2008), Argus *et al.* (2010) and Saria *et al.* (2014). The former two estimates predict opening velocities of 6.9–7.0 mm yr^{-1} towards N93.5-95.5°E in the Main Ethiopian Rift (black and brown vectors in Fig. 4b), close to the 7.6 mm yr^{-1}, N84°E velocity predicted by the Horner *et al.* (2007) 3.6-Myr average angular velocity.

In contrast, the more recent Saria *et al.* (2014) GPS angular velocity, which was derived from more GPS site velocities than earlier studies and incorporates the elastic effects of locked plate boundary faults during the inversion for the best-fitting angular velocity, predicts a significantly slower 4.8 ± 0.2 mm yr^{-1} (1σ) opening rate, but similar direction (N94°E ± 1.5°) (shown by the blue vector in Fig. 4b).

Our newly estimated Nubia–Somalia angular velocities, which span four distinct intervals during the past 3.6 Myr (Table 2), predict 4.2–5.0 mm yr^{-1} opening rates (Figs 3 and 4b), consistent with the

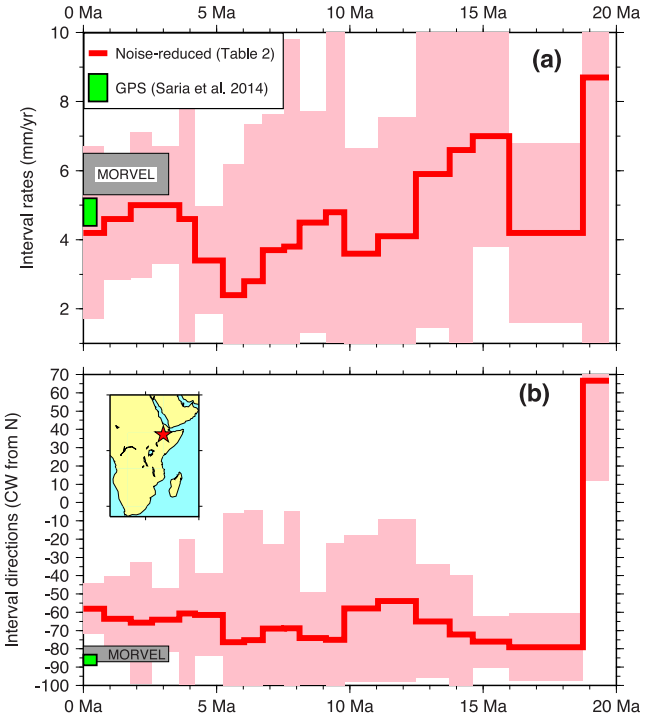

Figure 3. Nubia plate motion relative to Somalia plate, 20 Ma to present estimated from Southwest Indian Ridge data (red lines) described in Section 2. Interval rates (a) and directions (b) at 9°N, 40°E (star in inset map) estimated from the Table angular velocities. Velocities are also shown for the GPS-derived Nubia–Somalia angular velocity of Saria *et al.* (2014) and the MORVEL 3-Myr-average angular velocity (DeMets *et al.* 2010). The 1σ uncertainties in the latter two velocities are given by the vertical extents of the green and grey bars.

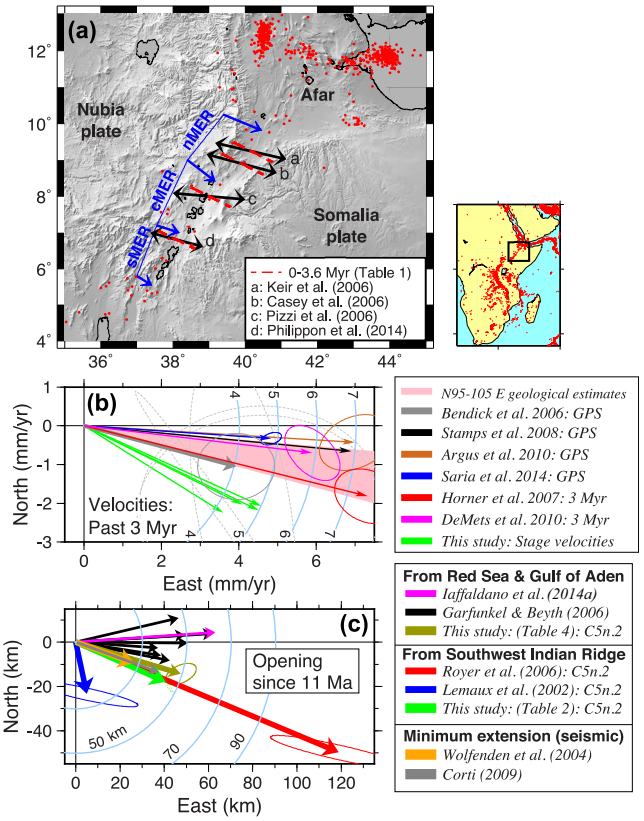

Figure 4. Geologic and plate kinematic estimates of opening along the Main Ethiopian Rift. (a) Location map. Black double-headed arrows labelled a–d show minimum principal stress directions estimated by sources given in the legend from (a) 36 earthquake focal mechanisms in the Main Ethiopian Rift, (b) the maximum elongation direction of three active rift volcanos, (c,d) fault plane and lineation palaeostress analysis. Dashed red lines show small circles about the 0–3.6 Myr Nubia–Somalia pole estimated herein (Table 1). Red circles show 1964–2014 earthquakes above 60 km and with magnitudes over 3.5. Blue arrows define the limits of the southern, central and northern segments of the Main Ethiopian Rift (abbreviated sMER, cMER and nMER, respectively). (b) Somalia plate velocities relative to the Nubia plate from this study, four GPS studies and two studies of 3-Myr-average plate motions (see legend). Green arrows show predicted velocities for the intervals between 0.0, 0.78, 1.778, 2.591 and 3.596 Ma (Table 1). (c) Cumulative Nubia–Somalia plate motion since 11 Ma. Black arrows are extrapolated from 0 to 10 Ma reconstructions of the Red Sea and the Gulf of Aden (table 2 of Garfunkel & Beyth 2006). Red and blue arrows are based on previous reconstructions of C5n.2 (11 Ma) along the Southwest Indian Ridge. Minimum rift-normal extensions estimated from seismically derived stretching factors are shown for the northern (grey arrow) and central (orange arrow) Main Ethiopian Rift (see the text). Velocities are predicted at 9.0°N, 40.0°E.

4.8 ± 0.2 mm yr^{-1} rate estimated with the Saria *et al.* (2014) GPS angular velocity. Together, they suggest that rates predicted by the older studies cited above are too fast.

At the same location, our new angular velocities predict N104-112°E opening directions (green arrows in Fig. 4b). These are rotated 10–30° clockwise from the geodetic and structural directions shown in Figs 4(a) and (b). For reasons given in Section 1 of the Supporting Information, we believe that this difference is an artefact of small errors in the DMS15 estimates of seafloor spreading rates along the Southwest Indian Ridge. We thus focus below on the implications of the more robustly determined rates.

3.3 Evidence for steady motion since 5.2 Ma

Fig. 5 shows the component of Nubia–Somalia motion orthogonal to the Main Ethiopian Rift as reconstructed with our new rotations. The reconstructed opening distances clearly suggest that the opening rate has been steady since at least 5.24 Ma. A regression of the six opening distances reconstructed for 0.78–5.24 Ma gives an average opening rate of 4.58 mm yr^{-1} and fits all six distances within their 1σ uncertainties. At the same location, the Saria *et al.* (2014) GPS angular velocity predicts a rift-normal opening component of 4.66 mm yr^{-1}, within 2 per cent of the 5.24-Myr average opening rate (compare red circles and black line in Fig. 5). The opening rate at the north end of the Nubia–Somalia plate boundary thus appears to have been steady since at least 5.2 Ma, in accord with the evidence for apparently steady opening directions during this period (Fig. 3b).

Between 11 Ma and 5.2 Ma, our new rotations predict rift-normal opening distances that are consistently smaller than the distances extrapolated from both the 5.24-Myr average best-fitting opening rate and the GPS estimate (Fig. 5). This may constitute evidence for a ≈25 per cent acceleration of the opening rate after ≈6 Ma, although we consider this possible change in motion to be uncomfortably close to the underlying scatter in the interval velocities (Fig. 3).

3.4 Reconstruction at 10.6 Ma

Fig. 6 depicts rift-normal opening distances across the northern segment of the Main Ethiopian Rift at 10.6 Ma as extrapolated from

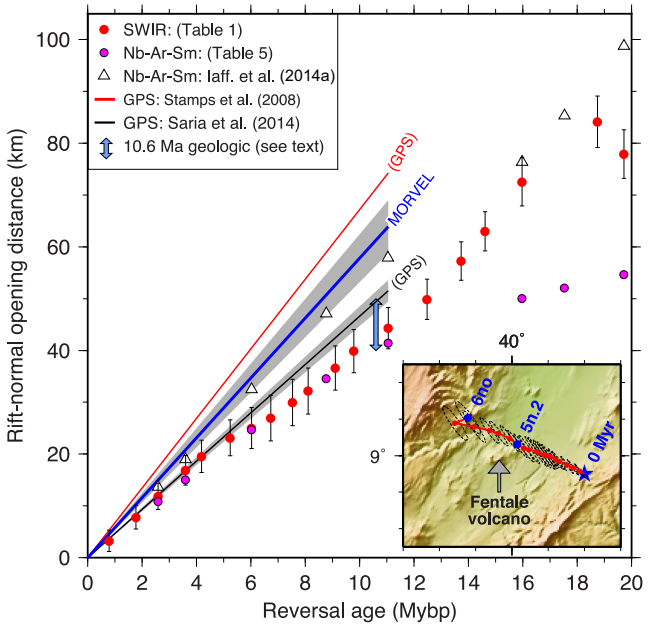

Figure 5. Rift-normal component of Nubia–Somalia plate motion at 9°N, 40°E along the Main Ethiopian Rift (inset map), 20 Ma to present. The plate displacements are rotated onto N70°W–S70°E, the direction orthogonal to the Main Ethiopian Rift. Displacements shown by the red circles were estimated using Table 1 rotations determined from reconstructions of the Southwest Indian Ridge (SWIR). Triangles and magenta circles show opening estimated from reconstructions of the Red Sea and Gulf of Aden for eight times since 20 Ma (Iaffaldano *et al.* 2014a and this study). The black, red and blue lines show extrapolations of the rift-normal opening distances back to 11 Ma based on linear velocities that are predicted by two, GPS-derived angular velocities and the MORVEL geological angular velocity (DeMets *et al.* 2010). All uncertainties are 1σ. The 0–20 Ma displacement path of the Somalia plate relative to Nubia (red and blue circles in the inset map) was reconstructed with the Table 1 rotations and is the basis for finding the rift-normal opening distances shown by the red circles in the main panel.

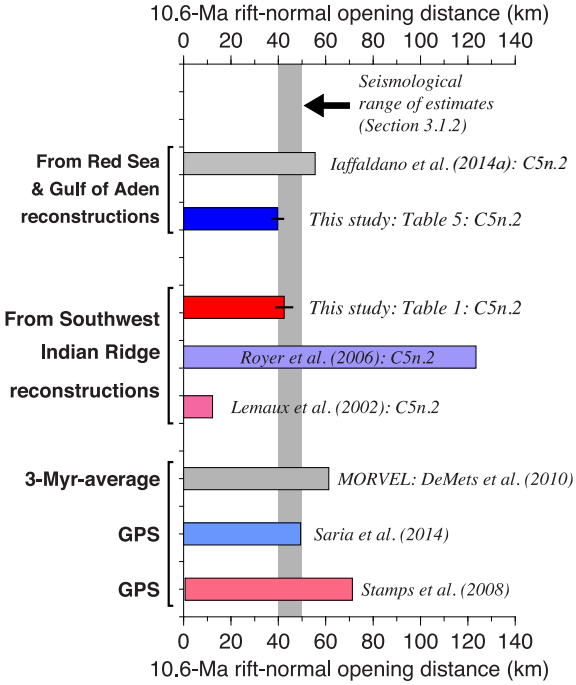

Figure 6. Estimates of the rift-normal (N70°W–S70°E) component of opening across the northern segment of the Main Ethiopian Rift at 10.6 Ma, when geologic data indicate the rift first opened (Wolfenden *et al.* 2004). The vertical grey bar spans the 40–50 km estimates of the cumulative opening across the northern rift segment based on detailed seismological surveys of the rift valley and assumptions about how much of the extension has been accommodated by normal faulting versus volcanic underplating and extrusion (see the text). The remaining estimates (horizontal bars) were estimated by extrapolating or interpolating Nubia–Somalia displacements predicted by rotations from this or previous studies to 10.6 Ma and projecting the predicted displacements onto the rift-normal direction.

the models cited above and estimated from seismologic and geological observations. The opening distance extrapolated to 10.6 Ma from Table 1 rotation for C5n.2 (11.06 Ma) is 42.5 ± 3.8 km (1σ). This agrees with the 40–50 km estimates of 10.6-Ma rift-normal extensions from dense broadband seismic surveys of the northern rift segment (Section 3.1.2). We interpret this as evidence that our Table 1 rotations for times back to at least 11.06 Ma are reliable. The good agreement between the plate kinematic and seismologic opening estimates also implies that extension between Nubia and Somalia at this location has been focused within the northern rift valley since it formed at ∼10.6 Ma.

3.5 Motion before 11 Ma

Nubia–Somalia plate reconstructions for times before 11.06 Ma are based on progressively fewer magnetic anomaly identifications from the Southwest Indian Ridge, particularly for the more sparsely mapped Nubia–Antarctic segment west of the Andrew Bain fracture zone, where the shipboard and airplane coverage of magnetic reversals older than ∼16 Ma is so sparse that some of the DMS15 magnetic anomaly identifications could be incorrect. Our confidence in the results for times older than ∼16 Ma is accordingly lower. Given that no previous authors have estimated Nubia–Somalia plate motion from magnetic reversals older than C5n.2 (11.06 Ma), there is no other basis of comparison for our newly estimated rotations.

Despite these concerns, our estimates of Nubia–Somalia motion before ≈10 Ma are generally well behaved (e.g. Fig. 5). For example, our reconstructions predict that the plate motion has been consistently orthogonal to the rift since 18.7 Ma (Fig. 7). The only interval during which the predicted motion was significantly oblique to the rift was from 19.7 to 18.7 Ma, the oldest interval spanned by our rotations and the interval in which we have the least confidence (also see Fig. 3b).

The 18.7-Myr finite rotation from Table 1 approximately reconstructs the present eastern margin of the Main Ethiopian Rift against its western margin (Fig. 7). Accommodating the predicted extension entirely within the present rift valley would require most or all of the extension to have occurred via the accretion of new lithosphere. This seems implausible in light of compelling geological evidence that normal faulting has accommodated significant extension within the Main Ethiopian Rift (e.g. Corti 2009 and references therein; Agostini *et al.* 2011). Structures outside the present rift valley thus must have accommodated motion between Nubia and Somalia before 10.6 Ma, when rifting initiated in this region (Wolfenden *et al.* 2004).

4 NUBIA–SOMALIA MOTION FROM THE NUBIA–ARABIA–SOMALIA PLATE CIRCUIT

As an independent check on the newly estimated Nubia–Somalia rotations in Table 1, we also estimated Nubia–Somalia plate motion

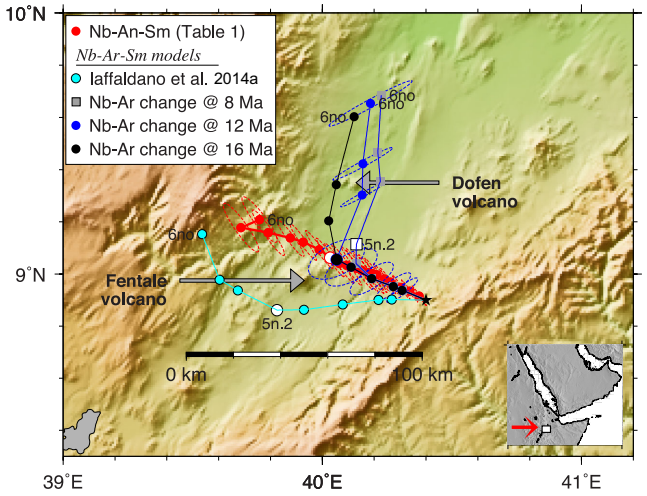

Figure 7. Reconstructed paths, present to 19.7 Ma, of a point on the Somalia plate relative to Nubia for the five models listed in the legend and described in the text. The lower three models listed in the legend variously assume that the motion between Nubia and Arabia across the Red Sea changed at 8, 12 or 16 Ma (Section 4). The inset map shows the location of the main map, which is centred on the Main Ethiopian Rift. The red symbols were reconstructed using Table 1 finite rotations based on data from the Southwest Indian Ridge, whereas the other symbols were reconstructed based on observations and constraints from Nubia–Arabia–Somalia plate circuit in the Red Sea and Gulf of Aden. For reference, the open symbols on each path mark the reconstruction for Chron 5n.2 (11.06 Ma).

from Somalia-Arabia and Nubia–Arabia rotations that respectively reconstruct the Gulf of Aden and Red Sea. Estimating rotations for the latter plate pair is challenging due to factors that include an absence of easily interpreted Red Sea magnetic anomalies older than ∼5 Ma, and significant uncertainties about the opening age of the Red Sea, the pole and angle that best close the Red Sea, and whether and when motion between Nubia and Arabia has changed. To cope with these uncertainties, we use a probabilistic method to identify the range of Nubia–Arabia plate kinematic models that simultaneously satisfy well-determined GPS constraints on recent Nubia–Arabia plate motion and broad constraints on the age and opening history of the Red Sea and the associated offsets of the Dead Sea Fault and normal faults in the Gulf of Suez (Garfunkel & Beyth 2006). Descriptions of our probabilistic assumptions, our results and a test of the estimated Nubia–Arabia rotations against geologic constraints from the Dead Sea and Gulf of Suez are found in the Supporting Information. The highlights of those results are presented briefly in Section 4.2.

4.1 Arabia–Somalia rotations and angular velocities

We derived rotations and angular velocities that describe Arabia–Somalia plate motion since 20 Ma (Tables 3 and 4) from a Bayesian analysis of a sequence of best-fitting rotations estimated by Fournier *et al.* (2010) from crossings of eight seafloor spreading magnetic reversals between Chrons 6n (19.72 Ma) and 2An.1 (2.58 Ma) in the Gulf of Aden. Although Iaffaldano *et al.* (2014a) previously applied their REDBACK noise-reduction software to the same sequence of best-fitting rotations, we elected to repeat their analysis with a more recent release of REDBACK (Version 1.0.4), which uses modified criteria to identify the least noisy sequence of finite rotations and angular velocities that are consistent with the constraints imposed by the best-fitting rotations.

Fig. 8 compares Arabia–Somalia interval rates and directions that are estimated with our newly determined, noise-reduced angular velocities (Table 4) and with angular velocities that we derived from Fournier *et al.*'s (2010) best-fitting rotations. As expected, the best-fitting velocities vary more erratically than do the noise-reduced velocities (compare red and dashed lines in Fig. 8). The interval rates and directions both appear to have remained steady since at least 6 Ma and possibly since 11 Ma, before which the rates were ∼20–40 per cent faster and the direction 10°–15° anticlockwise of the present direction. Within their uncertainties, the noise-reduced velocities during the past few Myr agree with those predicted by the MORVEL angular velocity, which spans the past 3 Myr (blue stippled region in Figs 8a and b). The noise-reduced rotations are used for the ensuing analysis.

4.2 Arabia–Nubia rotations

As is documented in Section 2 of the Supporting Information, we estimated Nubia–Arabia rotations using a probabilistic method that we designed to identify the full range of plausible kinematic models for Nubia–Arabia plate motion since 20 Ma. The key constraints and assumptions imposed during our analysis are as follows: (1) Motion during the most recent interval is constrained to equal the ArRajehi *et al.* (2010) GPS-derived Nubia–Arabia angular velocity. We also explored the consequences of forcing recent Nubia–Arabia plate motion to equal that specified by the Reilinger *et al.* (2006) GPS-derived Nubia–Arabia angular velocity. (2) The total opening of the Red Sea is variously constrained by six previously published Red Sea opening rotations, whose authors used differing assumptions about coastline matching and the nature of the lithosphere beneath the Red Sea to determine their preferred opening rotation. (3) The opening age of the Red Sea is assumed to be 24 ± 2 Ma, although

Table 3. Arabia–Somalia noise-reduced finite rotations.

Chron	Age (Ma)	Lat. (°N)	Long. (°E)	Ω (°)	Covariances					
					a	*b*	*c*	*d*	*e*	*f*
2An.1	2.581	23.75	25.39	1.086	1292.5	611.3	677.1	292.2	324.3	360.0
2An.3	3.596	23.76	25.47	1.516	1574.9	744.9	825.0	358.5	398.3	442.7
3An.1	6.033	23.86	25.62	2.538	2153.8	1022.4	1133.0	497.4	553.6	616.7
4Ay	8.771	23.84	25.87	3.762	2651.9	1259.3	1395.7	628.9	703.4	787.9
5n.2	11.056	24.20	25.79	4.704	2656.8	1250.9	1384.1	629.3	704.6	790.6
5Cn.1	15.974	25.38	24.79	6.730	2839.1	1283.6	1409.6	616.3	683.8	760.0
5Do	17.533	25.47	24.10	7.284	3782.3	1668.8	1825.0	771.6	850.8	939.6
6no	19.722	26.09	22.21	7.877	636.2	258.3	278.8	107.0	115.8	125.5

These rotations reconstruct movement of the Somalia plate relative to the Arabia plate and are determined from an analysis of best-fitting rotations in table 1 of Fournier *et al.* (2010) using REDBACK noise-reduction software (Iaffaldano *et al.* 2014b). Rotation angles Ω are positive anticlockwise. The Cartesian rotation covariances are calculated in a Somalia-fixed reference frame and have units of 10^{-9} radians^2. Elements *a*, *d* and *f* are the variances of the (0°N, 0°E), (0°N, 90°E) and 90°N components of the rotation. See footnotes to Table 1 for instructions on how to build the covariance matrix.

Table 4. Arabia–Somalia noise-reduced stage angular velocities.

Age(o) (Ma)	Age(y) (Ma)	Lat. (°N)	Long. (°E)	$\dot{\omega}$ (°)	Covariances					
					a	*b*	*c*	*d*	*e*	*f*
2.581	0.000	23.75	25.39	0.421	20.85	8.49	9.02	7.36	4.26	6.62
3.596	2.581	23.79	25.68	0.424	53.69	21.83	23.33	19.01	10.81	17.23
6.033	3.596	24.03	25.83	0.419	29.10	9.42	10.73	14.42	4.69	12.01
8.771	6.033	23.79	26.40	0.447	49.22	16.00	17.95	25.97	6.90	21.69
11.056	8.771	25.66	25.39	0.413	37.28	3.30	6.88	31.58	3.72	24.89
15.974	11.056	27.94	22.21	0.413	16.86	−1.29	1.73	17.92	1.39	12.78
17.533	15.974	25.90	15.68	0.358	118.81	1.69	25.40	128.97	−3.55	90.34
19.722	17.533	29.80	358.75	0.292	123.63	−8.08	35.01	157.14	−1.92	76.05

These angular velocities specify Arabia plate motion relative to the Somalia plate during the time period given in the first two columns, as determined from the REDBACK noise-reduction software (Iaffaldano *et al.* 2014b). The angular rotation rates $\dot{\omega}$ are positive anticlockwise for the old to the young limit of each time interval. The angular velocity covariances are calculated in a Somalia-fixed reference frame and have units of 10^{-8} radians^2 Myr^{-2}. See Table 1 footnotes for information on building the covariance matrix from elements *a* to *f*.

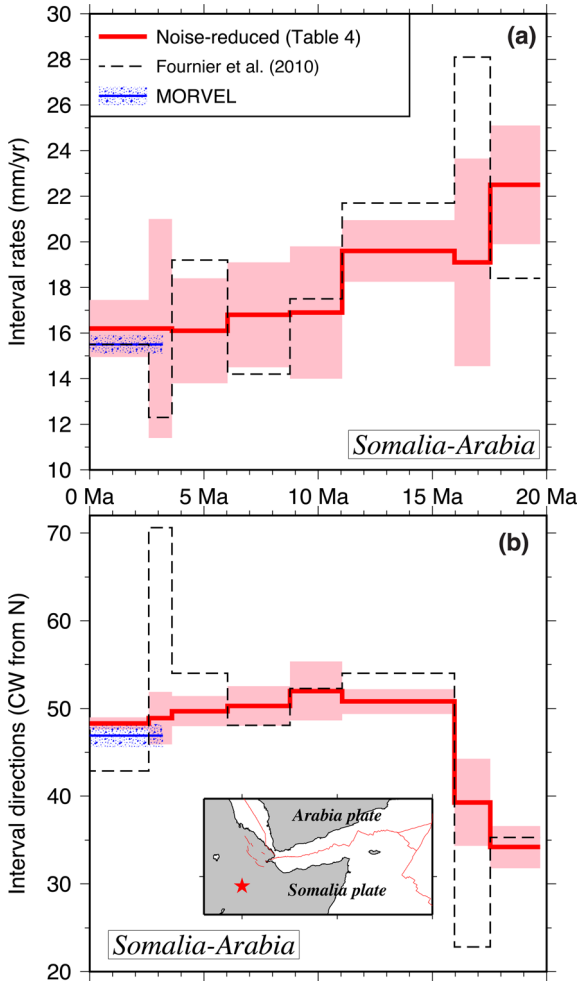

Figure 8. (a) Somalia–Arabia interval rates at 9°N, 40°E estimated from angular velocities based on sources given in the legend. The MORVEL angular velocity is from DeMets *et al.* (2010). (b) Somalia–Arabia interval directions from the same three sources.

we explored models that allowed opening to begin as early as 30 Ma. (4) Motion between Arabia and Nubia is required to be continuous and consist of either one or two periods of steady motion.

Based on our comparison of the results determined from our probabilistic analysis, including a determination of which results were consistent with geologic constraints imposed by the well-determined offsets of the Dead Sea Fault and normal faults in the Gulf of Suez, we elected to use the Red Sea opening rotation estimated by Joffe & Garfunkel (1987) to determine a preferred sequence of Nubia–Arabia rotations (Table 5). Further details are found in the Supporting Information.

Fig. 9 shows Nubia–Arabia interval rates and directions determined from a representative subset of the numerous two-stage opening models that we derived, including models in which the motion between Nubia and Arabia motion was allowed to change at 8 ± 0.2, 12 ± 0.2 or 16 ± 0.2 Ma. None of the numerous models sampled by our probabilistic method were consistent with a simple model in which both the direction and rate of opening across the Red Sea have remained constant between the onset of Red Sea rifting and the present. All of the models instead require that the Red Sea opening rate accelerated to its present, GPS-constrained rate after 24 ± 2 Ma, independent of the other assumptions and constraints that we applied during our analysis. Our preferred model suggests that the Red Sea opening direction has changed by no more than 4°–5° since 20 Ma (Fig. 9b).

4.3 Nubia–Somalia motion from closure of the Nubia–Arabia–Somalia circuit

We estimated Nubia–Somalia finite rotations from our Nubia–Arabia and Arabia–Somalia rotations in two stages. For each of the numerous, trial estimates of Nubia–Arabia plate motion from our probabilistic analysis, we first interpolated the Nubia–Arabia finite rotations to the eight times of the Arabia–Somalia rotations in Table 3. We then combined each sequence of interpolated Nubia–Arabia finite rotations with Table 3 Arabia–Somalia finite rotations to find a corresponding sequence of eight Nubia–Somalia finite rotations. The resulting distribution of Nubia–Somalia rotations implicitly satisfies the constraints that are imposed by the Gulf of Aden seafloor spreading history and the Nubia–Arabia opening constraints that are described in the Supporting Information.

4.3.1 Nubia–Somalia plate motion: 6 Ma to present

Nubia–Somalia stage poles for all three intervals within the past 6 Myr (i.e. 0–2.58, 2.58–3.60 and 3.60–6.03 Ma) are located in central and southern Africa (blue circles in Fig. 10) and predict opening directions across the Main Ethiopian Rift that are orthogonal to the rift (compare light blue and purple lines in Fig. 11b). The same three interval angular velocities predict 4.1–4.2 mm yr^{-1} opening rates since 6 Ma, in agreement with rates estimated from the observations along the Southwest Indian Ridge (red and purple

Table 5. Nubia–Arabia and Nubia–Somalia rotations.

Chron	Age (Ma)	Lat. (°N)	Long. (°E)	Ω (°)	Covariances *a*	*b*	*c*	*d*	*e*	*f*
Nubia–Arabia rotations										
2An.1	2.581	31.70	24.60	0.952	4.0	3.5	2.7	3.4	2.6	2.3
2An.3	3.596	31.70	24.60	1.327	7.7	6.8	5.3	6.6	5.0	4.4
3An.1	6.033	31.70	24.60	2.226	21.7	19.0	14.8	18.7	14.1	12.4
4Ay	8.771	31.70	24.60	3.237	45.9	40.2	31.3	39.5	29.8	26.2
5n.2	11.056	31.70	24.60	4.080	73.0	63.9	49.7	62.8	47.3	41.7
5Cn.1	15.974	31.70	24.60	5.894	152.3	133.5	103.9	131.2	98.8	87.0
5Do	17.533	31.77	24.70	6.255	1542.7	977.4	198.1	829.0	127.3	137.7
6no	19.722	31.86	24.81	6.761	1218.1	737.2	364.4	588.0	208.1	226.9
Nubia–Somalia rotations										
2An.1	2.581	−18.97	28.46	0.195	133.2	64.6	70.4	32.7	35.0	38.2
2An.3	3.596	−18.45	28.72	0.274	165.2	81.3	87.7	42.6	44.8	48.6
3An.1	6.033	−18.54	29.22	0.452	237.2	121.5	127.8	68.9	69.3	73.5
4Ay	8.771	−14.77	29.73	0.714	311.5	167.0	169.9	103.8	99.6	103.3
5n.2	11.056	−14.80	29.28	0.851	339.5	190.6	186.2	128.2	116.7	117.4
5Cn.1	15.974	−11.28	23.61	1.087	440.3	266.5	239.4	198.7	163.2	153.0
5Do	17.533	−7.06	19.59	1.269	1908.1	1146.0	370.3	925.9	206.1	224.6
6no	19.722	−3.64	9.22	1.367	1275.9	770.8	378.3	615.0	214.4	229.0

The Nubia–Arabia rotations reconstruct the Nubia plate onto Arabia at the times listed in Column 2. The rotations and rotation covariances for Chrons 2An.1 to 5Cn.1 were extrapolated from the GPS angular velocity estimate of ArRajehi *et al.* (2010). The rotations for Chrons 5D and 6no were interpolated between the 24-Myr-to-present Red Sea opening rotation of Joffe & Garfunkel (1987) and a 16-Myr-to-present rotation extrapolated from the GPS-based angular velocity. The covariances for Chrons 5D and 6no were approximated assuming 1-D, 1σ circular reconstruction uncertainties of ±5 km for the Joffe & Garfunkel 24-Ma-to-present Red Sea opening rotation and scaling the covariances to the ages of Chrons 5D and 6n. The Nubia–Somalia rotations, which reconstruct the Somalia plate onto Nubia plate, are estimated from the Arabia–Somalia noise-reduced rotations in Table 3 and Nubia– Arabia finite rotations listed above. Rotation angles Ω are positive anticlockwise. The Cartesian rotation covariances are calculated in a Somalia-fixed reference frame and have units of 10^{-8} radians^2. Footnotes to Table 1 give further information about the covariances.

lines in Fig. 11a) and the 4.8 ± 0.2 mm yr^{-1} rate predicted by the Saria *et al.* (2014) GPS angular velocity. If we substitute the Reilinger *et al.* (2006) GPS-derived Nubia–Arabia angular velocity for the ArRajehi *et al.* (2010) angular velocity that was used for our Nubia–Arabia probabilistic analysis and repeat the probabilistic analysis to derive modified estimates for Nubia–Arabia and Nubia–Somalia plate motions, the predicted Nubia–Somalia interval rates for the past 6.03 Ma increase to 4.75 mm yr^{-1}, close to the 4.8 ± 0.2 mm yr^{-1} GPS estimate and consistent with the 5.2-Myr average estimates from the Southwest Indian Ridge data.

We interpret the good agreement between these independent estimates as evidence that Nubia–Somalia plate motion has been steady since at least 5.2 Ma.

4.3.2 Nubia–Somalia plate motion before 6 Ma

Our numerous probabilistic estimates of Nubia–Somalia plate motion before 6 Ma include models that permit changes in Nubia–Arabia plate motion as recently as 6 Ma or as early as 18 Ma. For simplicity, we focus below on the subset of solutions for which Nubia–Arabia plate motion changed at either 8 ± 0.2, 12 ± 0.2 or 16 ± 0.2 Ma (Figs 10 and 11). These are representative of the range of solutions we examined.

All of our probabilistic solutions predict that Nubia–Somalia motion has significantly exceeded zero for the past 20 Myr (Fig. 11a), irrespective of when and if Nubia–Arabia plate motion changed, when the Red Sea began opening and the opening model that we adopt for the Red Sea. It thus appears that motion between the two plates initiated before 20 Ma, consistent with the evidence for non-zero motion back to at least 18.7 Ma from the Southwest Indian Ridge data. Rates between the two plates at the northern end of the East African Rift have averaged 3–7 mm yr^{-1} for the past 16 Ma (Fig. 11a), irrespective of the age that is assumed for a change in Red Sea opening velocities.

Extrapolating our Table 5 C5n.2 Nubia–Somalia rotation to 10.6 Ma and projecting the displacement onto the direction orthogonal to the Main Ethiopian Rift gives 39.8 ± 2.5 km of rift-normal extension (Figs 5 and 6). Substituting the Reilinger *et al.* (2006) GPS-derived Nubia–Arabia angular velocity for the ArRajehi *et al.* (2010) angular velocity and repeating the calculation increases the predicted rift-normal opening to 47.6 ± 2.7 km. Both agree with the 40–50 km, seismologically derived estimate and thus implicitly suggest that Nubia–Arabia motion has been steady or nearly steady since at least 10.6 Ma.

Nubia–Somalia stage poles for times that predate the assumed change in Nubia–Arabia plate motion are located significantly northwest of the stage poles for times since 11 Ma and far north of similar-age stage poles estimated from data along the Southwest Indian Ridge (Fig. 10). Random or systematic errors in subsets of the data and/or constraints that were used to estimate each set of stage poles must be the source of the difference. For example, if we substitute the Reilinger *et al.* (2006) GPS-derived Nubia–Arabia angular velocity for the ArRajehi *et al.* (2010) angular velocity used for the analysis above and repeat our probabilistic analysis of Nubia–Arabia and Nubia–Somalia plate motions, the Nubia–Somalia stage poles for times before 11 Ma move roughly 10° to the south and are significantly closer to the poles based on the Southwest Indian Ridge data than are the stage poles estimated with the ArRajehi *et al.* GPS angular velocity. The large difference in the stage poles is perhaps surprising given that the Red Sea opening rates and directions predicted by the Reilinger *et al.* (2006) Nubia–Arabia angular velocity differ from those estimated with the ArRajehi *et al.* angular velocity by only 0.5–0.9 mm yr^{-1} and 0.6°–0.9°. This underlines the sensitivity of the stage pole locations to even small changes in the GPS-derived angular velocities. By inference, small errors in any

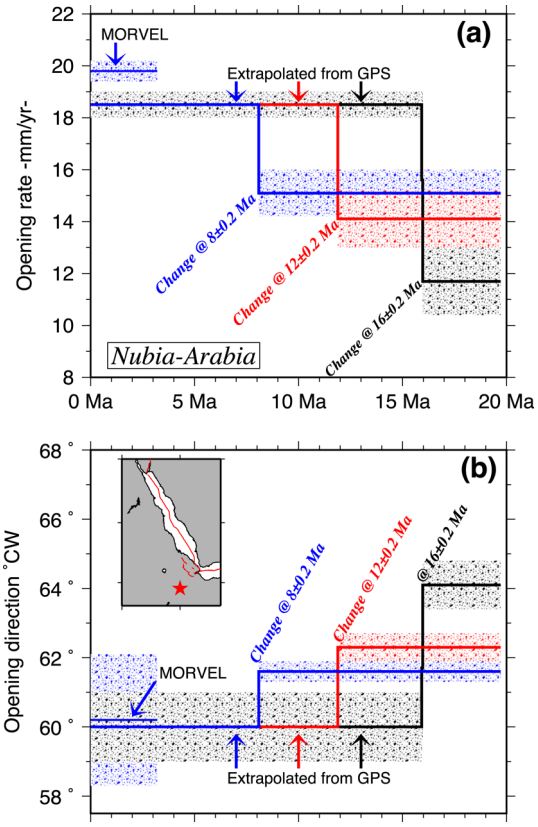

Figure 9. Nubia–Arabia interval rates (panel a) and directions (panel b) and their 1σ uncertainties at 9°N, 40°E in the Ethiopian Rift (star in inset map) estimated from the MORVEL angular velocity (DeMets *et al.* 2010) and from three subsets of the probabilistic models described in the text and Supporting Information. The subsets include all of the realizations of Nubia–Arabia plate motion for which the motion changes at 8 ± 0.2 Ma (blue line), 12 ± 0.2 Ma (red line) or 16 ± 0.2 Ma (black line) (see legend). The bold lines and their associated stippled areas show the average rate or direction per solution subset and their 1σ scatters.

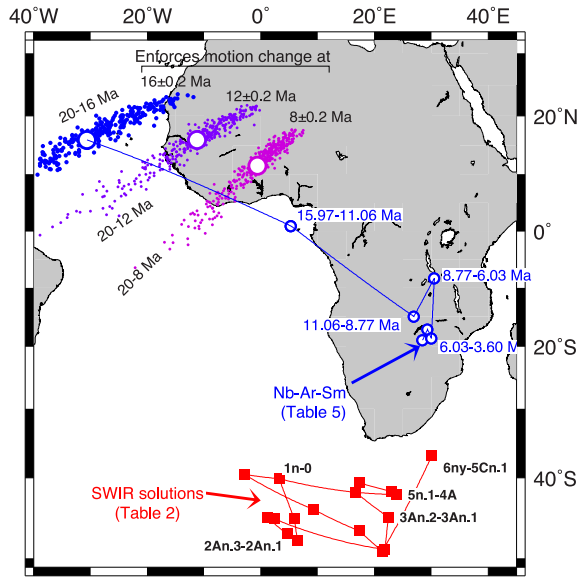

Figure 10. Nubia–Somalia stage poles, 0–20 Ma. Red squares show poles determined from Southwest Indian Ridge angular velocities in Table 2. Blue circles show stage poles based on Table 5 rotations, which were determined from analyses of Gulf of Aden and Red Sea rotations described in Section 4 and the Supporting Information. These were derived assuming motion between Nubia and Arabia changed at 16 Ma (see the text). Alternative estimates in which Nubia–Arabia motion was assumed to have changed at 8 or 12 Ma are also shown. Large open circles show averages of the 20–8 Ma, 20–12 Ma and 20–16 Ma stage pole distributions.

of the Fournier *et al.* (2010) Arabia–Somalia reconstructions may also significantly impact our Nubia–Somalia rotation estimates.

For the reasons outlined above, we are skeptical of the kinematic evidence for highly oblique Nubia–Somalia motion at times before ∼10 Ma on the basis of reconstructions of the opening histories of the Red Sea and Gulf of Aden.

5 DISCUSSION

5.1 Nubia–Somalia plate motion since 20 Ma

The Nubia–Somalia rotations and angular velocities determined from the DMS15 Southwest Indian Ridge reconstructions and from data and constraints in the Red Sea and Gulf of Aden both indicate that the two plates have rotated around a stationary pole (Figs 2b and 12) at a steady angular rotation rate since at least 5.2 Ma. In particular, the opening distances predicted by six Nubia–Somalia finite rotations derived from the Southwest Indian Ridge rotations (Table 1) have changed linearly since 5.2 Ma (Fig. 5). The rate that best fits the rift-normal components of those six opening distances, 4.58 ± 0.1 mm yr^{-1} (1σ), differs by only 2 per cent from the 4.66 ± 0.2 mm yr^{-1} rift-normal opening rate predicted by the GPS-derived Nubia–Somalia angular velocity of Saria *et al.* (2014) and by less than 10 per cent from the 4.2 ± 0.2 mm yr^{-1} rift-normal opening rate that best fits the 2.58, 3.60 and 6.03 Myr opening distances estimated from closure of the Nubia–Arabia–Somalia plate circuit (Section 4.3.1).

Spanning the past 11 Myr, our Nubia–Somalia motion estimates allow for two possible scenarios, one in which motion increased ≈25 per cent at ∼6–5.2 Ma and the other in which motion has remained steady for the entire time. In support of the former, opening distances that are reconstructed with rotations determined from the Southwest Indian Ridge data (Table 1) are consistently smaller for times before 5.2 Ma than opening distances extrapolated to older times based on our 5.2-Myr-to-present Table 1 rotations or extrapolated from the Saria *et al.* (2014) GPS angular velocity (Fig. 5). The uncertainties in our seismologically based estimate of opening across the Main Ethiopian Rift (the double-headed blue arrow in Fig. 5) are large enough however to permit an alternative interpretation, namely, that our Table 1 rotations modestly underestimate the cumulative extension between 5.2 and 10.6 Ma and that Nubia–Somalia motion from 10.6 to 5.2 Ma was the same as for 5.2 Ma to the present.

For times before ≈11 Ma, the predictions of significantly faster and more oblique motion by both sets of rotations (Fig. 11) warrant skepticism. The rotations determined from closure of the Nubia–Arabia–Somalia plate circuit, are sensitive to small errors in estimates of Arabia–Somalia rotations and generally predict that plate motion was highly oblique to the present plate boundary at all times before 11 Ma (Fig. 7). This disagrees with flow lines reconstructed with rotations from the Southwest Indian Ridge data (red symbols in Fig. 7) and rotations from Iaffaldano *et al.* (2014a), who used different constraints from the Gulf of Aden and Red Sea to estimate Nubia–Somalia rotations (light blue symbols in Fig. 7). We reiterate that the accuracy and temporal resolution of our results for times before 16 Ma are compromised by sparse coverage of magnetic

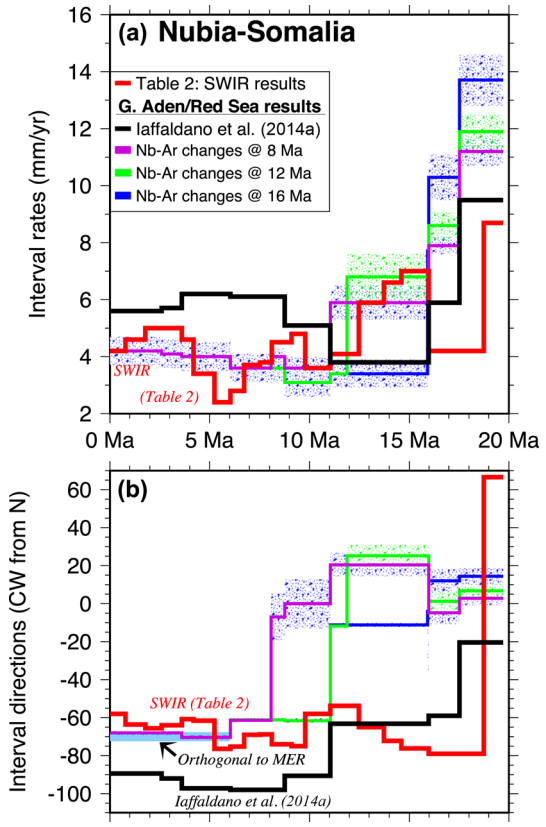

Figure 11. Nubia–Somalia interval rates (panel a) and directions (panel b), 20 Ma to present, predicted at 9.0°N, 40.0°E. The Table 2 angular velocities are based on reconstructions of Southwest Indian Ridge (SWIR) data, whereas all the other angular velocities were derived from finite rotations that reconstruct data from the Gulf of Aden and Red Sea. Estimates of Nubia–Somalia motion that are based on our numerous, probabilistic estimates of Nubia–Arabia motion (Section 4.2) are limited to the subsets of the estimates for Nubia–Arabia plate motion that are permitted to change at 8 ± 0.2 Ma (purple line), 12 ± 0.2 Ma (green line), or 16 ± 0.2 Ma (blue line) (see legend). The light blue area in panel (b) shows the direction orthogonal to the Main Ethiopian Rift (MER). The bold lines and their associated stippled areas show the average solutions and 1σ scatters for each of the three solution subsets. Abbreviations: Ar, Arabia; Nb, Nubia; Sm, Somalia.

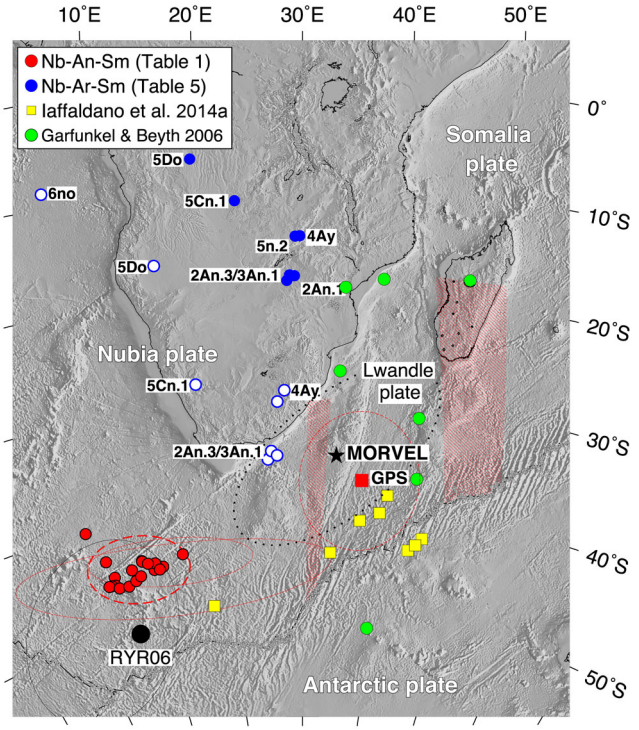

Figure 12. Nubia–Somalia finite opening poles for models discussed in the text. Red circles show poles determined from the REDBACK analysis of the Nubia–Antarctica and Somalia–Antarctica rotations of DeMets *et al.* (2015). Poles labelled 'GPS', 'MORVEL' and 'RYR06' are from Saria *et al.* (2014), DeMets *et al.* (2010) and Royer *et al.* (2006), respectively. The DeMets *et al.* (2010) and Royer *et al.* (2006) opening poles specify Nubia-Somalia plate motion over the past 3.0 Ma and 11.0 Ma, respectively. Poles from table 2 of Garfunkel & Beyth (2006), Iaffaldano *et al.* (2014a) and Table 5 of this study (blue) are estimated from rotations that reconstruct the Red Sea and Gulf of Aden (e.g. the Nubia–Arabia–Somalia plate circuit). Poles located by the open blue circles were estimated by substituting the Reilinger *et al.* (2006) GPS estimate of Nubia–Arabia motion for the ArRajehi *et al.* (2010) GPS estimate and repeating the probabilistic analysis described in the text and Supporting Information. Uncertainty ellipses are 2-D, 95 per cent ; the Chron 6n ellipses are dashed. The red-patterned areas north of the Southwest Indian Ridge approximate the best locations of the likely diffuse boundaries that define the east and west edges of the Lwandle plate (Horner-Johnson *et al.* 2007; DeMets *et al.* 2015). Earthquakes are for the period 1964–2013, are limited to magnitudes greater than 3.5 and depths above 60 km (www.neic.cr.usgs.gov).

reversals older than C5Cn.1 along the western third of the Southwest Indian Ridge. More reliable estimates of Nubia–Somalia plate motion before 16 Ma will require (at minimum) well-navigated, modern surveys of magnetic reversals older than Chron 5 on both sides of the western third of the Southwest Indian Ridge.

5.2 Comparison to previous studies

Nubia–Somalia rotations estimated by previous authors from reconstructions of Southwest Indian Ridge data differ significantly from our own. In particular, 11.06-Ma finite rotations estimated by Lemaux *et al.* (2002) and Royer *et al.* (2006) from reconstructions of Chron 5n.2 predict respective Somalia plate displacements of 24 ± 7 km, S12°E ± 36° and 129 ± 22 km, S67°E ± 2° in the Main Ethiopian Rift. Extrapolating these to the 10.6 Ma opening age of the rift and projecting them onto the rift-normal direction gives respective predicted extensions of 12 ± 13 and 123 ± 14 km (Fig. 6). These differ from each other by an order-of-magnitude and disagree with 42.5 ± 3.8 and 39.8 ± 2.5 km 10.6-Myr rift-normal opening components extrapolated from our C5n.2 rotations in Tables 1 and 5. The direction of motion since 11.06 Ma predicted by the Lemaux *et al.* (2002) rotation also differs significantly from all other estimates (blue arrow in Fig. 4c).

Our analysis confirms, but refines conclusions reached by Garfunkel & Beyth (2006), who estimate seven different 10-Myr Nubia–Somalia finite rotations (green circles in Fig. 12) based on different combinations of Arabia–Somalia and Nubia–Arabia finite rotations that satisfy a range of geologic and kinematic constraints from the central and northern Red Sea and Gulf of Aden. Their Nubia–Somalia finite-opening poles, which are generally located south of Africa, but east of our estimates (green and blue circles in Fig. 12), predict opening directions across the East Africa Rift that are 5°–15° anticlockwise from the directions predicted by our newly estimated rotations (Fig. 4c). Extrapolations to 10.6 Ma of the extension that is predicted by their 10-Myr finite rotations across the northern Main Ethiopian Rift give 36–61 km of cumulative opening, similar to our own estimates.

Iaffaldano *et al.* (2014a) estimate Nubia–Somalia rotations for eight times during the past 20 Myr from sequences of Arabia–Somalia and Nubia–Arabia rotations that they derived using the REDBACK Bayesian methodology (yellow squares in Fig. 12). A flow line reconstructed with their rotations is located systematically south of flow lines we reconstructed using our own rotations (Fig. 7). Interval rates and directions estimated with angular velocities we determined from their rotations are consistently faster than and anti-clockwise from those predicted by our own angular velocities (Fig. 11). We interpret this as further evidence that estimates of Nubia–Somalia motion based on constraints from the Red Sea and Gulf of Aden are sensitive to differences between the data and assumptions that are used by different authors to arrive at those estimates.

Fig. 12 summarizes Nubia–Somalia pole locations from most of the studies cited herein for times ranging from the present (GPS) to 20 Ma. One pattern that emerges from a comparison of these poles is the tendency for poles from individual studies to cluster near each other, but far from the poles estimated in other studies. We attribute this to the sensitivity of the estimated pole locations to the assumptions and observations that are used by the authors of the different studies, including our own. A simple exercise illustrates this point. If we substitute the Reilinger *et al.* (2006) GPS estimate of Nubia–Arabia plate motion for the ArRajehi *et al.* (2010) GPS estimate that is otherwise used for our probabilistic analysis, the resulting Nubia–Somalia poles (shown by the open blue circles in Fig. 12) are shifted 10 degrees south of their counterparts. Better geodetic and marine geophysical data are needed to identify and correct for small data biases that are most likely the cause of the differences in these estimates.

Finally, we attribute the modest differences between the velocities that are predicted by our new Nubia–Somalia angular velocities (green arrows in Fig. 4b) and the 3-Myr-average MORVEL angular velocity (DeMets *et al.* 2010) to a combination of factors that include the different plate circuit closure constraints that are satisfied by MORVEL versus our new estimates, the different calibrations that are used by DeMets *et al.* (2010) and DMS15 to compensate for outward displacement along the Nubia–Antarctic segment of the Southwest Indian Ridge, and differences between the two studies in where the Lwandle–Somalia plate boundary is assumed to intersect the Southwest Indian Ridge.

6 CONCLUSIONS

Nubia–Somalia finite and stage rotations that are derived from the Nubia–Antarctic and Somalia-Antarctic segments of the Southwest Indian Ridge are used to describe for the first time Nubia–Somalia plate motion at ∼1-Myr intervals since 20 Ma. Six rotations that describe motion from the present back to 5.24 Myr predict an average rate of rift-normal extension across the Main Ethiopian Rift that agrees within ± 2 per cent with that estimated with GPS (Saria *et al.* 2014), and also predict rift-normal extensions that are consistent with those predicted by Nubia–Somalia rotations estimated from closure of the Nubia–Arabia–Somalia plate circuit. Extrapolating the rift-normal extensions predicted by our 11.06 Ma finite rotation to 10.6 Ma, the opening age of the northern segment of the Main Ethiopian Rift, gives net extension of 42.5 ± 3.8 km, consistent with the 40–50 km of extension estimated from seismic surveys. The predictions of our new rotations are thus validated at multiple time scales for the past ∼11 Myr.

The new Nubia–Somalia rotations also suggest that the two plates have been in relative motion for all of the past 20 Myr, but suggest that motion during the oldest times modelled herein (∼20–16 Ma) may have been highly oblique to the present rift valleys of eastern Africa. The rotations for older times are derived from many fewer observations than for times since 11 Myr and are accordingly less certain. Improved survey coverage of magnetic reversals older than Chron 5 along the western half of the Southwest Indian Ridge would greatly improve the basis for evaluating the magnitude and significance of Nubia–Somalia motion before ∼16 Ma.

New estimates of Nubia–Somalia rotations determined from Arabia–Somalia rotations and Nubia–Arabia rotations that span a wide range of possible Red Sea opening histories corroborate our results based on data from the Southwest Indian Ridge, particularly for the past 11 Myr. Stage poles that describe Nubia–Somalia motion before ∼11 Ma differ significantly in location when determined from closures of the Nubia–Arabia–Somalia versus the Nubia–Antarctic–Somalia plate circuits. Although the source of this discrepancy is unresolved, large uncertainties in the rotations that describe the pre-16-Myr relative motions of the plate pairs within these two three-plate circuits are the most likely cause.

ACKNOWLEDGEMENTS

We thank Giacomo Corti and Cindy Ebinger for useful suggestions at various stages during the preparation of this manuscript, and Cindy Ebinger, the associate editor Duncan Agnew and an anonymous reviewer for suggestions that significantly improved the original manuscript. This work was supported by grants OCE-0926274 and OCE-1433323 from the U.S. National Science Foundation. Figures were drafted using Generic Mapping Tools software (Wessel & Smith 1991).

REFERENCES

Abebe, T., Balestrieri, M.L. & Bigazzi, G., 2010. The Central Main Ethiopian Rift is younger than 8 Ma: Confirmation through apatite fission-track thermochronology, *Terra Nova,* **22,** 470–476.

Agostini, A., Bonini, M., Corti, G., Sani, F. & Manetti, P., 2011. Distribution of Quaternary deformation in the central Main Ethiopian Rift, East Africa, *Tectonics,* **30,** TC4010, doi:10.1029/2010TC002833.

Argus, D.F., Gordon, R.G., Heflin, M.B., Ma, C., Eanes, R., Willis, P., Peltier, W.R. & Owen, S.E., 2010. The angular velocities of the plates and the velocity of Earth's centre from space geodesy, *Geophys. J. Int.,* **180**(3), 913–960.

ArRajehi, A. *et al.*, 2010. Geodetic constraints on present-day motion of the Arabian plate: implications for Red Sea and Gulf of Aden rifting, *Tectonics,* **29,** TC3011, doi:10.1029/2009TC002482.

Bendick, R., McClusky, S., Bilham, R., Asfaw, L. & Klemperer, S., 2006. Distributed Nubia-Somalia relative motion and dike intrusion in the Main Ethiopian Rift, *Geophys. J. Int.,* **165,** 303–310.

Bonini, M., Corti, G., Innocenti, F., Manetti, P., Mazzarini, F., Abebe, T. & Pecskay, Z., 2005. Evolution of the Main Ethiopian Rift in the frame of Afar and Kenya rifts propagation, *Tectonics,* **24,** TC1007, doi:10.1029/2004TC001680.

Bosworth, W. & McClay, K., 2001. Structural and stratigraphic evolution of the Gulf of Suez Rift, Egypt: a synthesis, in *Peri-Tethys Memoir 6: Peri-Tethyan Rift/Wrench Basins and Passive Margins,* Vol. 186, pp. 567–606, eds Ziegler, P.A., Cavazza, E.W., Robertson, A.H.F. & Crasquin-Soleau, S., Museum National d'Histoire naturelle de Paris.

Bosworth, W., Huchon, P. & McClay, K., 2005. The Red Sea and Gulf of Aden Basins, *J. Afr. Earth Sci.,* **43,** 334–378.

Cande, S.C., Patriat, P. & Dyment, J., 2010. Motion between the Indian, Antarctic, and African plates in the early Cenozoic, *Geophys. J. Int.,* **183,** 127–149.

Casey, M., Ebinger, C.J., Keir, D., Gloaguen, R. & Mohamad, F., 2006. Strain accommodation in transitional rifts: extension by magma intrusion and faulting in Ethiopian rift magmatic segments, in *The Afar Volcanic Province within the East African Rift System,* Vol. 259, pp. 143–163, eds Yirgu, G., Ebinger, C.J. & Maguire, P.K.H., Geological Society Special Publication, Geological Society.

Chu, D. & Gordon, R.G., 1999. Evidence for motion between Nubia and Somalia along the Southwest Indian Ridge, *Nature,* **398,** 64–67.

Cochran, J.R., 1983. A model for the development of the Red Sea, *Am. Assoc. Pet. Geol. Bull.,* **67,** 41–69.

Cornwell, D.G., Maguire, P.K.H., England, R.W. & Stuart, G.W., 2010. Imaging detailed crustal structure and magmatic intrusion across the Ethiopian Rift using a dense linear broadband array, *Geochem. Geophys. Geosyst.,* **11,** Q0AB03, doi:10.1029/2009GC002637.

Corti, G., 2009. Continental rift evolution: from rift initiation to incipient break-up in the Main Ethiopian Rift, East Africa, *Earth-Sci. Rev.,* **96,** 1–53.

Corti, G., Sani, F., Philippon, M., Sokoutis, D., Willingshofer, E. & Molin, P., 2013. Quaternary volcano-tectonic activity in the Soddo region, western margin of the Southern Main Ethiopian Rift, *Tectonics,* **32,** 861–879.

DeMets, C., Gordon, R.G., Argus, D.F. & Stein, S., 1990. Current plate motions, *Geophys. J. Int.,* **101,** 425–478.

DeMets, C., Gordon, R.G. & Argus, D.F., 2010. Geologically current plate motions, *Geophys. J. Int.,* **181,** 1–80.

DeMets, C., Merkouriev, S. & Sauter, D., 2015. High-resolution estimates of Southwest Indian Ridge plate motions, 20 Ma to present, *Geophys. J. Int.,* **203,** 1495–1527.

Dyment, J., Tapponnier, P., Affi, A.M., Zinger, M.A., Franken, D. & Muzaiyen, E., 2013. A new seafloor spreading model of the Red Sea: magnetic anomalies and plate kinematics, Abstract T21A-2512 presented at *the 2013 Fall Meeting*, AGU, San Francisco, CA, 9–13 December.

Ebinger, C.J. & Casey, M., 2001. Continental breakup in magmatic provinces: an Ethiopian example, *Geology,* **29,** 527–530.

Fournier, M. *et al.*, 2010. Arabia-Somalia plate kinematics, evolution of the Aden-Owen-Carlsberg triple junction, and opening of the Gulf of Aden, *J. geophys. Res.,* **115,** doi:10.1029/2008JB006257.

Freund, R., 1970. Plate tectonics of the Red Sea and East Africa, *Nature,* **228,** 453–453.

Garfunkel, Z. & Beyth, M., 2006. Constraints on the structural development of Afar imposed by the kinematics of the major surrounding plates, in *The Afar Volcanic Province within the East African Rift System,* Vol. 259, pp. 23–42, eds Yirgu, G., Ebinger, C.J. & Maguire, P.K.H., Geological Society Special Publication, Geological Society.

Hayward, N.J. & Ebinger, C.J., 1996. Variations in the along-axis segmentation of the Afar Rift system, *Tectonics,* **15,** 244–257.

Hilgen, F.J., Lourens, L.J. & Van Dam, J.A., 2012. The Neogene Period, in *The Geologic Time Scale 2012,* pp. 923–978, eds Gradstein, F.M., Ogg, J.G., Schmitz, M. & Ogg, G., Elsevier.

Horner-Johnson, B.C., Gordon, R.G., Cowles, S.M. & Argus, D.F., 2005. The angular velocity of Nubia relative to Somalia and the location of the Nubia–Somalia–Antarctica triple junction, *Geophys. J. Int.,* **162,** 221–234.

Horner-Johnson, B.C., Gordon, R.G. & Argus, D.F., 2007. Plate kinematic evidence for the existence of a distinct plate between the Nubian and Somalian plates along the Southwest Indian Ridge, *J. geophys. Res.,* **112,** B05418, doi:10292006JB004519.

Iaffaldano, G., Bodin, T. & Sambridge, M., 2012. Reconstructing plate-motion changes in the presence of finite-rotations noise, *Nat. Commun.,* **3,** 1048, doi:10.1038/ncomms2051.

Iaffaldano, G., Hawkins, R. & Sambridge, M., 2014a. Bayesian noise-reduction in Arabia/Somalia and Nubia/Arabia finite rotations since ∼20 Ma: implications for Nubia/Somalia relative motion, *Geochem. Geophys. Geosyst.,* **15,** 845–854.

Iaffaldano, G., Hawkins, R., Bodin, T. & Sambridge, M., 2014b. REDBACK: open-source software for efficient noise-reduction in plate kinematic reconstructions, *Geochem. Geophys. Geosyst.,* **15,** 1663–1670.

Izzeldin, A., 1987. Seismic, gravity, and magnetic surveys in the central part of the Red Sea: their interpretation and implications for the structure and evolution of the Red Sea, *Tectonophysics,* **143,** 269–306.

Jestin, F., Huchon, P. & Gaulier, J.M., 1994. The Somalia plate and the East African Rift System: present-day kinematics, *Geophys. J. Int.,* **116,** 637–654.

Joffe, S. & Garfunkel, Z., 1987. Plate kinematics of the circum-Red Sea - A re-evaluation, *Tectonophysics,* **141,** 5–22.

Keir, D., Ebinger, C.J., Stuart, G.W., Daly, E. & Ayele, A., 2006. Strain accommodation by magmatism and faulting as rifting proceeds to breakup: Seismicity of the northern Ethiopian rift, *J. geophys. Res.,* **111,** B05314, doi:10.1029/2005JB003748.

Keranen, K. & Klemperer, S.L., 2008. Discontinuous and diachronous evolution of the Main Ethiopian Rift: implications for development of continental rifts, *Earth planet. Sci. Lett.,* **265,** 96–111.

Keranen, K., Klemperer, S.L., Gloaguen, R. & EAGLE Working Group 2004. Three-dimensional seismic imaging of a protoridge axis in the Main Ethiopian Rift, *Geology,* **32,** 949–952.

Kirkwood, B.H., Royer, J.-Y., Chang, T.C. & Gordon, R.G., 1999. Statistical tools for estimating and combining finite rotations and their uncertainties, *Geophys. J. Int.,* **137,** 408–428.

Lemaux, J., Gordon, R.G. & Royer, J.-Y., 2002. Location of the Nubia-Somalia boundary along the Southwest Indian Ridge, *Geology,* **30,** 339–342.

Le Pichon, X. & Francheteau, J., 1978. A plate tectonic analysis of the Red SeaGulf of Aden area, *Tectonophysics,* **46,** 369–406.

Maguire, P.K.H. *et al.*, 2006. Crustal structure of the Northern Main Ethiopian Rift from the EAGLE controlled source survey: a snapshot of incipient lithospheric break-up, in *The Afar Volcanic Province within the East African Rift System,* Vol. 259, pp. 23–42, eds Yirgu, G., Ebinger, C.J. & Maguire, P.K.H., Geological Society Special Publication, Geological Society.

McKenzie, D.P., Davies, D. & Molnar, P., 1970. Plate tectonics of the Red Sea and East Africa, *Nature,* **226,** 243–248.

McQuarrie, N., Stock, J.M., Verdel, C. & Wernicke, B.P., 2003. Cenozoic evolution of Neotethys and implications for the causes of plate motions, *Geophys. Res. Lett.,* **30**(20), 2036, doi:10.1029/2003GL017992.

Merkouriev, S. & DeMets, C., 2014. High-resolution estimates of Nubia-North America plate motion: 20 Ma to present, *Geophys. J. Int.,* **196,** 1281–1298.

Minster, J.B. & Jordan, T.H., 1978. Present-day plate motions, *J. geophys. Res.,* **83,** 5331–5354.

Minster, J.B., Jordan, T.H., Molnar, P. & Haines, E., 1974. Numerical modeling of instantaneous plate tectonics, *Geophys. J. R. astr. Soc.,* **36,** 541–576.

Mohr, P.A., 1970. Plate tectonics of the Red Sea and east Africa, *Nature,* **228,** 547–548.

Ogg, J.G., 2012. Geomagnetic polarity time scale, in *The Geologic Time Scale 2012,* pp. 85–113, eds Gradstein, F.M., Ogg, J.G., Schmitz, M. & Ogg, G., Elsevier.

Patriat, P., Sloan, H. & Sauter, D., 2008. From slow to ultraslow: a previously undetected event at the Southwest Indian Ridge at ca. 24 Ma, *Geology,* **36,** 207–210.

Philippon, M. *et al.*, 2014. Evolution, distribution, and characteristics of rifting in southern Ethiopia, *Tectonics,* **33,** doi:10.1002/2013T003430.

Pizzi, A., Coltorti, M., Abebe, B., Disperati, L., Sacchi, G. & Salvini, R., 2006. The Winji fault belt (main Ethiopian Rift): Structural and geomorphological constraints and GPS monitoring, in *The Afar Volcanic Province within the East African Rift System,* Vol. 259, pp. 192–207, eds Yirgu, G., Ebinger, C.J. & Maguire, P.K.H., Geological Society Special Publication, Geological Society.

Reilinger, R. & McClusky, S., 2011. Nubia-Arabia-Eurasia plate motions and the dynamics of Mediterranean and Middle East tectonics, *Geophys. J. Int.,* **186,** 971–979.

Reilinger, R., McClusky, S., Vernant, P., Lawrence, S. & many others 2006. GPS constraints on continental deformation in the Africa-Arabia-Eurasia continental collision zone and implications for the dynamics of plate interactions, *J. geophys. Res.,* **111,** B05411, doi:10.10292005JB004051.

Roeser, H.A., 1975. A detailed magnetic survey of the southern Red Sea, *Geol. Jahrb.,* **D13,** 131–153.

Rosenbaum, G., Lister, G.S. & Duboz, C., 2002. Relative motions of Africa, Iberia, and Europe during the Alpine orogeny, *Tectonophysics,* **359,** 117–129.

Royer, J.-Y., Gordon, R.G. & Horner-Johnson, B.C., 2006. Motion of Nubia relative to Antarctica since 11 Ma: implications for Nubia–Somalia, Pacific-North America, and India-Eurasia motion, *Geology,* **34,** 501–504.

Saria, E., Calais, E., Stamps, D.S., Delvaux, D. & Hartnady, C.J.H., 2014. Present-day kinematics of the East African Rift, *J. geophys. Res.,* **119,** 3584–3600.

Stamps, D.S., Calais, E., Saria, E., Hartnady, C., Nocquet, J.-M., Ebinger, C.J. & Fernandes, R.M., 2008. A kinematic model for the East African Rift, *Geophy. Res. Lett.,* **35,** L05304, doi:10.1029/2007GL032781.

Sultan, M., Becker, R., Arvidson, R.E., Shore, P., Stern, R.J., Alfy, Z. El & Guinness, E.A., 1992. Nature of the Red Sea crust: a controversy revisited, *Geology,* **20,** 593–596.

Wessel, P. & Smith, W.H.F., 1991. Free software helps map and display data, *EOS, Trans. Am. geophys. Un.,* **72,** 441–446.

Wolfenden, E., Ebinger, C., Yirgu, G., Deino, A. & Ayalew, D., 2004. Evolution of the northern Main Ethiopian rift: birth of a triple junction, *Earth planet. Sci. Lett.,* **224,** 213–228.

Wolfenden, E., Ebinger, C., Yirgu, G., Renne, P.R. & Kelley, S.P., 2005. Evolution of a volcanic rifted margin: Southern Red Sea, Ethiopia, *Bull. geol. Soc. Am.,* **117,** 846–864.

SUPPORTING INFORMATION

Additional Supporting Information may be found in the online version of this paper:

Table S1. Nubia–Somalia best-fitting rotations from Southwest Indian Ridge

Figure S1. Linear velocities for the Nubia–Arabia–Somalia (a) and Nubia–Antarctica–Somalia (b) plate circuits estimated at 9°N, 40°E from the 3.16-Myr-average MORVEL angular velocities (DeMets *et al*. 2010). (c) Trade-off between speed-ups or slowdowns in the Arabia–Somalia rate and the Nubia–Somalia velocity magnitude and orientation at 9°N, 40°E. Changes of only ±1 mm yr^{-1} in the Arabia–Somalia rate (horizontal axis) cause changes as large as 10° in the Nubia–Somalia direction (red line) when closure of the velocity circuit shown in (a) is enforced. To first-order, the same tradeoffs exist for changes in the Arabia–Nubia rate. (d) Sensitivities of the predicted Nubia–Somalia rate and direction to small speed-ups or slowdowns in the Antarctica–Somalia rate. Nearly the same tradeoffs exist for changes in the Antarctica–Nubia rate. For the Nubia–Antarctica–Somalia plate circuit, the estimated Nubia–Somalia rate is relatively insensitive to errors in the estimated Nubia–Antarctica or Somalia-Antarctica rates.

Figure S2. Probability density functions (PDF) used to construct trial models for the history of Nubia–Arabia (Nb–Ar) motion across the Red Sea. (a–f) Present-day (GPS), total-opening, and stage poles that constrain Red Sea opening per model tested. Open square locates the GPS pole of ArRajehi *et al*. (2010). Blue symbols show total opening pole estimates, with abbreviations as follows 'McK70' McKenzie *et al*. (1970); 'Sltn92' Sultan *et al*. (1992); 'JG87' Joffe & Garfunkel (1987); 'LPG88' Le Pichon & Gaulier (1988); 'GB-Rt2' 'GB-Rt3' from table 3 of Garfunkel & Beyth (2006). Red circles show Nubia–Arabia stage poles that describe opening from the time that the Red Sea opened until the time that motion is assumed to have changed (see text). Arabia–Somalia poles from Table 3 are shown in (c) and (d). The methods used to determine the acceptable (Gaussian) limits on the total opening poles (and opening angles, which are not shown), are described in the text. (g) Distribution of ages at which Nubia–Arabia plate motion is assumed to have changed. These are limited to ages between 6 and 18 Ma. (h) Distribution of ages at which opening of the Red Sea is assumed to have occurred. These are limited to ages between 22 and 26 Ma. Results for ten thousand independent trial estimates for each of the above models are shown.

Figure S3. Nubia–Arabia opening rates (a & c) and directions (b & d) based on Red Sea opening rotations estimated by Joffe & Garfunkel (1987) and Sultan *et al*. (1992). The estimates based on these two models are end-member results amongst the six published models described in the text and shown in Fig. S2a–f. Estimates of Nubia–Arabia plate motion are derived by assuming two intervals of constant plate motion since the Red Sea opened. As described in the text, motion during the younger interval is defined by a rotation that is extrapolated from GPS (see text) and motion during the older interval is defined by a stage rotation that is estimated from the difference between the younger rotation and the assumed total opening rotation for the Red Sea. The age when Nubia–Arabia motion changed and the age that opening commenced across the Red Sea are treated as unknowns and are drawn from probability distribution functions shown in Fig. S2gh. Results from 10,000 trial models are illustrated. Velocities are calculated at 9.0°N, 40.0°E.

Figure S4. Comparison of Nubia–Arabia velocities between the Dead Sea Fault in the north and Main Ethiopian Rift in the south as predicted by the older-interval and younger-interval angular velocities determined from the probabilistic analysis described in Section 3 of the main document. The velocities labeled 'GPS' in both panels are predicted by the GPS-derived Nubia–Arabia angular velocity of ArRajehi *et al*. (2010), which is assumed to be representative of Nubia–Arabia motion during the younger (recent) interval. The older-interval velocities, variously labeled '20–16 Myr' etc., assume that opening of the Red Sea started at 24 Ma and that plate motion variously changed at 12 Myr, 14 Myr, or 16 Myr. The older-interval rotations in Panels A and B are constrained to consistency with the Joffe & Garfunkel (1987) and Sultan *et al*. (1992) Red Sea opening rotations, respectively.

Figure S5. Test of end-member Red Sea (Nubia–Arabia) opening models against geological slip estimates for the Dead Sea Fault and normal faults in the Gulf of Suez (labeled DSF and GS respectively in the inset map). Panel A shows the predicted displacement of Nubia relative to the Arabia plate at 19.7 Ma reduced by 105 km of post-20-Myr left-lateral slip along the N17.5°E-trending Dead Sea Fault (Garfunkel 2014). The Nubia–Arabia displacements are predicted at a location along the Dead Sea Fault using probabilistic estimates based on the Joffe & Garfunkel (1987) and Sultan *et al*. (1992) estimates (see text). The residual movement shown in Panel A was presumably accommodated partly or wholly by normal faulting across the Gulf of Suez. Open circles show the average of each distribution. In Panel B, the residual movements from Panel A are rotated onto axes that trend N55°E and N35°W, which are orthogonal and parallel to the trend of normal faults in and along the Gulf of Suez. The grey area shows 15–36 km structural estimates of the total extension across normal faults in the northern and southern Gulf of Suez (Bosworth & McClay 2001). Abbreviations: AR, Arabia plate; NB, Nubia plate; SN, Sinai microplate.

Figure S6. Motion of Nubia relative to Somalia plate, 20 Ma to present. (a) and (c) show interval rates and (b) and (d) show

interval directions that are predicted at 9.0°N, 40.0°E by stage rotations determined from the rotations in Tables 1 and 4, from our probability-density-function (PDF) analysis, and from Iaffaldano *et al*. (2014a). Stage rotations labeled 'SWIR' are determined from the finite rotations in Table 1 of the main document, which are based on reconstructions of data from the Southwest Indian Ridge (SWIR). Stage rotations from the latter three sources are determined from finite rotations that reconstruct data from the Gulf of Aden and Red Sea. Grey and other colored regions show the range of interval velocities derived by combining the Somalia-Arabia noise-reduced rotations in Table 3 with ten thousand Nubia–Arabia trial rotations that were derived from the probability density function (PDF) analysis described in the text. Probabilistic velocity estimates are propagated from the Joffe & Garfunkel (1987) Red Sea (Nubia–Arabia) opening rotation.
(http://gji.oxfordjournals.org/lookup/suppl/doi:10.1093/gji/ggw276/-/DC1)

Please note: Oxford University Press is not responsible for the content or functionality of any supporting materials supplied by the authors. Any queries (other than missing material) should be directed to the corresponding author for the paper.